A Hybrid High-Order method for the mixed Steklov eigenvalue problem

ROMMEL BUSTINZA*, MATTEO CICUTTIN † and ARIEL L. LOMBARDI‡

Abstract

In this paper we discuss the approximation of the spectrum of the Steklov eigenvalue problem, by using the well known Hybrid High-Order (HHO) method. The analysis developed in this work is partially based on the existing literature about the HHO method for the Laplacian eigenvalue problem. As usual with HHO methods, we are able to eliminate the volume unknowns, by introducing a suitable discrete solver operator. This allows us to numerically solve on the skeleton of the mesh, reducing the computational cost. The a priori error analysis lets us to prove optimal convergence rates for the eigenvalues and the eigenfunctions, when the latter are smooth enough. Numerical examples that confirm our theoretical findings are provided.

Keywords: Steklov eigenvalue problem; Hybrid high-order method; a priori error analysis; Polytopal meshes.

1 Introduction

The Steklov eigenvalue problem arises in a multitude of mathematical and engineering contexts, such as in the dynamic of liquids in moving containers, known as the sloshing problem [28]. We can also mention the mechanical oscillators immersed in a viscous fluid [37], and the vibration modes of a structure in contact with an incompressible fluid [9].

The importance of the numerical solution of the Steklov problem is clear from the literature, where various conforming Finite Element approaches are documented at least since the end of the seventies: one of the earliest works is found in [10]; more recent FEM approaches are found for example in [6] and [32]. In the last few years however, interest has shifted on nonconforming and hybrid discretizations of the Steklov eigenvalue problem HDG [34]

Hybrid methods were introduced to mitigate the high number of unknowns generated by the classical Discontinuous Galerkin (DG) method, while retaining its advantages like full polyhedral support and arbitrary polynomial order. Very informally, hybrid methods define some element-local problem in each mesh element and subsequently couple them via face unknowns only: in this way one obtains a global problem posed in terms of face-based unknowns only, contrary to DG which yields a global problem posed in terms of cell-based unknowns. Since unknowns of the global problem are face-based, this class of methods is also known as Discontinuous Skeletal (DS) methods.

A recent development in the family of Discontinuous Skeletal methods is the Hybrid High-Order method (HHO in the following) [27, 26]. The main features of HHO are the approximation of the

*Corresponding author. Centro de Investigación en Ingeniería Matemática (CI^{2}MA) and Departamento de Ingeniería Matemática, Universidad de Concepción, Concepción, Chile, e-mail: rbustinza@udec.cl

†Dipartimento di Scienze Matematiche, Politecnico di Torino, Torino, Italy, e-mail: matteo.cicuttin@polito.it

‡Departamento de Matemática, Facultad de Ciencias Exactas, Ingeniería y Agrimensura, Universidad Nacional de Rosario, Rosario, Argentina, e-mail: ariel@fceia.unr.edu.ar

solution with arbitrary order polynomials, support for fully polyhedral meshes and easy hp-refinement. In addition, HHO methods are constructed independently from the geometric dimension and the element shape, allowing fully generic [18] software implementations. In HHO the unknowns are placed both in the cells and on the faces of the mesh, in order to approximate a pair including the primal variable in the cells and its trace on the skeleton. In particular, these unknowns are used by (i) a reconstruction operator, which reconstructs a high-order field in the cell and (ii) by a stabilization operator, which weakly enforces in each mesh cell the matching of the traces of the cell functions with the face unknowns. These two operators are then combined in a local bilinear form which, after local static condensation, is assembled into a global problem posed only on the face unknowns.

HHO methods have been used extensively mainly in the context of computational mechanics, for example solid mechanics [1, 2, 3], contact problems [16], obstacle problems [19] and fluid mechanics [15, 11]. Recent applications include acoustic time-dependent wave problems[12, 13], magnetostatics [17], and time-harmonic Maxwell equations [20]. In addition, HHO has been used for the solution of elliptic eigenvalue problems in [14].

Bridges and unifying viewpoints between HHO and other DS methods have progressively emerged. One of the most important connections was established in [22], where HHO methods were embedded in the Hybrid Discontinuous Galerkin (HDG) framework [23, 24]. Differently from HHO, HDG approximates a triple including the primal variable, its trace and the dual variable, in addition the analysis of the two methods relies on different theoretical ingredients. Weak Galerkin [40] (WG) methods were bridged to HDG in [21] and therefore they are also closely related to HHO. HHO and WG were developed independently, but they share the common point of view of combining a reconstruction (called weak gradient in WG) and a stabilization. HHO however employs a more sophisticated stabilization which allows to achieve higher convergence rates. In [22], also a connection to the nonconforming Virtual Element Method [7] was established.

In this work we are interested in devising an HHO method to solve the Steklov eigenvalue problem. The rest of the paper is organized as follows. In Section 2 we introduce the Steklov eigenvalue problem, discussing its primal variational formulation at continuous level. Moreover, a relationship among the referred eigenvalues and the spectrum of the so-called "solver operator", are established. Next, the HHO framework is described in Section 3, deducing the corresponding discrete scheme for the Steklov eigenvalue problem. Adapting ideas from a previous HHO work [14], we are able to find a finite-rank linear solver operator, establishing similar relationships among the spectrum of the operator and the eigenvalues of Steklov model. The convergence properties of the developed HHO method are discussed in Section 4. Several numerical examples are shown in Section 5, whose results are in agreement with our theoretical analysis.

2 Eigenvalue model problem

Let Ω be a bounded and simply connected domain in $\mathbb{R}^d$, $d \in \{2, 3\}$, with Lipschitz continuous boundary $\Gamma := \partial\Omega$. We allow that $\Gamma = \overline{\Gamma}_{\mathtt{S}} \cup \overline{\Gamma}_{\mathtt{N}} \cup \overline{\Gamma}_{\mathtt{R}}$, with $\Gamma_{\mathtt{S}}$, $\Gamma_{\mathtt{N}}$, $\Gamma_{\mathtt{R}}$ being disjoint open subsets of $\partial\Omega$ and $|\Gamma_{\mathtt{S}}|, |\Gamma_{\mathtt{R}}| > 0$. By $\boldsymbol{n}$ we denote the unit outward normal to Γ. We are interested in the mixed Steklov eigenvalue problem: *Find eingenpair* (λ, u) such that

$$\begin{cases} -\Delta u = 0 & \text{in} \quad \Omega\,, \\ \nabla u \cdot \boldsymbol{n} = \lambda\, u & \text{on} \quad \Gamma_{\mathtt{S}}\,, \\ \nabla u \cdot \boldsymbol{n} = 0 & \text{on} \quad \Gamma_{\mathtt{N}}\,, \\ \nabla u \cdot \boldsymbol{n} + \alpha\, u = 0 & \text{on} \quad \Gamma_{\mathtt{R}}\,, \end{cases} \tag{1}$$

where α is a positive constant function. With the aim of deriving a coercive primal variational formulation, we rewrite the first boundary condition in (1) as

$$\nabla u \cdot \boldsymbol{n} + u = (\lambda + 1)\, u \quad \text{on} \quad \Gamma_{\mathtt{S}}\,. \tag{2}$$

Remark 2.1 *In the present case performing the shift is not strictly necessary. However, we consider it in order to give a final theoretical remark later.*

Then, it is not difficult to deduce the weak formulation: *Find the eigenpair* $(\lambda, u) \in \mathbb{R} \times H^1(\Omega)$*, such that*

$$(\nabla u, \nabla v)_{0,\Omega} + (\alpha\, u, v)_{0,\Gamma_{\mathtt{R}}} + (u, v)_{0,\Gamma_{\mathtt{S}}} = (\lambda + 1)\,(u, v)_{0,\Gamma_{\mathtt{S}}} \quad \forall\, v \in H^1(\Omega)\,. \tag{3}$$

This allows us to introduce the solver operator $K : L^2(\Gamma_{\mathtt{S}}) \to L^2(\Gamma_{\mathtt{S}})$, such that for a given $g \in L^2(\Gamma_{\mathtt{S}})$, $K(g) := \gamma(z(g))|_{\Gamma_{\mathtt{S}}}$, where γ denotes the usual trace operator from $H^1(\Omega)$ onto $H^{1/2}(\Gamma)$, and $z(g) \in H^1(\Omega)$ is the unique solution of the so-called *source problem*:

$$a(z(g), v) = (g, v)_{0,\Gamma_{\mathtt{S}}} \quad \forall\, v \in H^1(\Omega)\,, \tag{4}$$

where $a : H^1(\Omega) \times H^1(\Omega) \to \mathbb{R}$ is the bilinear form given by

$$a(w, v) := (\nabla w, \nabla v)_{0,\Omega} + (\alpha\, w, v)_{0,\Gamma_{\mathtt{R}}} + (w, v)_{0,\Gamma_{\mathtt{S}}} \quad \forall\, w, v \in H^1(\Omega)\,.$$

It is not difficult to prove that a is symmetric, bounded and coercive on $H^1(\Omega)$. For the latter property, we take into account the Generalized Poincaré inequality. As a consequence, we now are interested in solving the eigenvalue problem: *Find the eigenpair* $(\mu, z) \in \mathbb{C} \times L^2(\Gamma_{\mathtt{S}})$ such that $K(z) = \mu\, z$. We recall the following result, that relates the eigenvalue pairs of (2) and K.

Lemma 2.1 *The operator K is compact, self-adjoint, and if (λ, u) is a eigenpair of* (1)*, then $\left(\frac{1}{\lambda+1}, \gamma(u)|_{\Gamma_{\mathtt{S}}}\right)$ is an eigenpair of K. Moreover, the eigenvalues of* (1) *are positive, isolated and diverge to infinity.*

Proof. The proof follows the ideas given in the proofs of Lemmas 2.1 and 2.2 in [34]. We omit further details. □

3 The HHO method for the eigenvalue problem

We introduce a shape-regular polytopal mesh family $\mathcal{S} := \{\mathcal{T}_h\}_{h>0}$, in the sense described in [25]. As expected, each element $\mathcal{T}_h$ of $\mathcal{S}$ is a partition of $\overline{\Omega}$ made of non-overlapping polytopal elements. By $\mathcal{F}_h^{\mathtt{int}}$ we denote the collection of interior faces inherited by $\mathcal{T}_h$, and by $\mathcal{F}_h^{\partial\Omega}$ we represent the collection of boundary faces. Then, the skeleton induced by $\mathcal{T}_h$ is denoted by $\mathcal{F}_h = \mathcal{F}_h^{\mathtt{int}} \cup \mathcal{F}_h^{\partial\Omega}$. In addition, we decomposed $\mathcal{F}_h^{\partial\Omega}$ as the non-overlapping union $\mathcal{F}_h^{\mathtt{S}} \cup \mathcal{F}_h^{\mathtt{N}} \cup \mathcal{F}_h^{\mathtt{R}}$, where for $j \in \{\mathtt{S}, \mathtt{N}, \mathtt{R}\}$, $\mathcal{F}_h^j$ represents the collection of boundary faces lying on Γ_j. Moreover, for any $\emptyset \neq A \subset \mathbb{R}^d$, with $d \in \{2, 3\}$, $h_A := \mathrm{diam}(A)$. On the other hand, given $T \in \mathcal{T}_h$, we set $\mathcal{F}_T := \{F \in \mathcal{F}_h : F \subset \partial T\}$ as the collection of boundary faces of element T. For each $F \in \mathcal{T}$, $\boldsymbol{n}_{TF}$ denotes the unit normal to F pointing out of T. Finally, the mesh size of $\mathcal{T}_h$ is defined as $h := \max_{T \in \mathcal{T}_h} h_T$.

For any integer $k \geq 0$ and $r \in \{d-1, d\}$, $\mathcal{P}_r^k(S)$ denotes the space of real-valued polynomials of total degree at most k on the r-dimensional affine manifold $S \subseteq \mathbb{R}^d$. We introduce the local discrete HHO approximation space

$$\underline{\boldsymbol{U}}_T^k := \left\{ \underline{\boldsymbol{v}}_T := (v_T, (v_F)_{F \in \mathcal{F}_T}) \in \mathcal{P}_d^k(T) \times \prod_{F \in \mathcal{F}_T} \mathcal{P}_{d-1}^k(F) \right\}.$$

In addition, the global discrete HHO approximation space is given by

$$\underline{\boldsymbol{U}}_h^k := \left\{ \underline{\boldsymbol{v}}_h := \Big((v_T)_{T \in \mathcal{T}_h}, (v_F)_{F \in \mathcal{F}_h} \Big) \in \prod_{T \in \mathcal{T}_h} \mathcal{P}_d^k(T) \times \prod_{F \in \mathcal{F}_h} \mathcal{P}_{d-1}^k(F) \right\}.$$

Next, we introduce the standard seminorm on $\underline{\boldsymbol{U}}_T^k$

$$|||\underline{\boldsymbol{v}}_T|||_{1,T}^2 := ||\nabla v_T||_{0,T}^2 + |\underline{\boldsymbol{v}}_T|_{0,\mathcal{F}_T}^2, \quad \forall\, \underline{\boldsymbol{v}}_T \in \underline{\boldsymbol{U}}_T^k, \tag{5}$$

where $|\underline{\boldsymbol{v}}_T|_{0,\mathcal{F}_T}^2 := \sum_{F \in \mathcal{F}_T} h_T^{-1} ||v_F - v_T||_{0,F}^2$. This allows us to define the usual seminorm on $\underline{\boldsymbol{U}}_h^k$

$$|||\underline{\boldsymbol{v}}_h|||_{1,h}^2 := \sum_{T \in \mathcal{T}_h} |||\underline{\boldsymbol{v}}_T|||_{1,T}^2, \quad \forall\, \underline{\boldsymbol{v}}_h \in \underline{\boldsymbol{U}}_h^k. \tag{6}$$

Now, given $\underline{\boldsymbol{v}}_h := \Big((v_T)_{T \in \mathcal{T}_h}, (v_F)_{F \in \mathcal{F}_h} \Big) \in \underline{\boldsymbol{U}}_h^k$, by v_h we denote the function belonging to $L^2(\Omega)$, such that $\forall\, T \in \mathcal{T}_h : v_h|_T := v_T$. In addition, by $\gamma_h(\underline{\boldsymbol{v}}_h)$ we represent the discrete trace of $\underline{\boldsymbol{v}}_h$ on $\mathcal{F}_h^{\partial\Omega}$, such that $\forall\, F \in \mathcal{F}_h^{\partial\Omega} : \gamma_h(\underline{\boldsymbol{v}}_h)|_F := v_F$.

Then, it is not difficult to check that the map: $||\cdot||_h : \underline{\boldsymbol{U}}_h^k \to \mathbb{R}$, such that $\forall\, \underline{\boldsymbol{v}}_h \in \underline{\boldsymbol{U}}_h^k : ||\underline{\boldsymbol{v}}_h||_h^2 := |||\underline{\boldsymbol{v}}_h|||_{1,h}^2 + ||\gamma_h(\underline{\boldsymbol{v}}_h)||_{0,\Gamma_{\mathtt{S}}}^2 + ||\alpha^{1/2}\gamma_h(\underline{\boldsymbol{v}}_h)||_{0,\Gamma_{\mathtt{R}}}^2$, defines a norm on $\underline{\boldsymbol{U}}_h^k$.

In order to devise the HHO method, a local reconstruction operator and a suitable local stabilization operator are needed. Given any $T \in \mathcal{T}_h$, we introduce the local reconstruction operator $p_T^{k+1} : \underline{\boldsymbol{U}}_T^k \to \mathcal{P}_d^{k+1}(T)$ such that for each $\underline{\boldsymbol{v}}_T := (v_T, (v_F)_{F \in \mathcal{F}_T}) \in \underline{\boldsymbol{U}}_T^k$, we have

$$\begin{cases} (\nabla p_T^{k+1}(\underline{\boldsymbol{v}}_T), \nabla w)_T = (\nabla v_T, \nabla w)_T + \sum_{F \in \mathcal{F}_T} (\nabla w \cdot \boldsymbol{n}_{TF}, v_F - v_T)_F \quad \forall\, w \in \mathcal{P}_d^{k+1}(T) \\ (p_T^{k+1}(\underline{\boldsymbol{v}}_T) - v_T, 1)_T = 0\,. \end{cases}$$

In addition, we set the global reconstruction operator $p_h^{k+1} : \underline{\boldsymbol{U}}_h^k \to \mathcal{P}_d^{k+1}(\mathcal{T}_h)$, such that $\forall\, T \in \mathcal{T}_h : \forall\, \underline{\boldsymbol{v}}_h \in \underline{\boldsymbol{U}}_h^k : p_h^{k+1}(\underline{\boldsymbol{v}}_h)|_T := p_T^{k+1}(\underline{\boldsymbol{v}}_T)$.

The local stabilization operator $S_{\partial T}^k : \underline{\boldsymbol{U}}_T^k \to \mathcal{P}_{d-1}^{k+1}(\mathcal{F}_T)$ is given such that for each $\underline{\boldsymbol{v}}_T := (v_T, (v_F)_{F \in \mathcal{F}_T}) \in \underline{\boldsymbol{U}}_T^k$, we have

$$S_{\partial T}^k(\underline{\boldsymbol{v}}_T) := \Pi_{\partial T}^k(v_{\partial T} - p_T^{k+1}(\underline{\boldsymbol{v}}_T)|_{\partial T}) \,-\, \Pi_T^k(v_T - p_T^{k+1}(\underline{\boldsymbol{v}}_T))|_{\partial T}\,,$$

with Π_T^k and $\Pi_{\partial T}^k$ representing the usual L^2-orthogonal projectors from $L^1(T)$ onto $\mathcal{P}_d^k(T)$ and from $L^1(\partial T)$ onto $\mathcal{P}_{d-1}^k(\mathcal{F}_T)$, respectively. We also introduce the global stabilization operator $s_h : \underline{\boldsymbol{U}}_h^k \times \underline{\boldsymbol{U}}_h^k \to \mathbb{R}$, given by

$$\forall\, \underline{\boldsymbol{v}}_h, \underline{\boldsymbol{w}}_h \in \underline{\boldsymbol{U}}_h^k : s_h(\underline{\boldsymbol{v}}_h, \underline{\boldsymbol{w}}_h) := \sum_{T \in \mathcal{T}_h} (\tau_{\partial T} S_{\partial T}^k(\underline{\boldsymbol{v}}_T), S_{\partial T}^k(\underline{\boldsymbol{w}}_T))_{\partial T}\,,$$

with $\tau_{\partial T} \in \mathcal{P}_0(\mathcal{F}_T)$ such that $\forall\, F \in \mathcal{F}_T : \tau_{\partial T}|_F = \eta\, h_T^{-1}$, and $\eta > 0$ at our disposal. Usually, $\eta := 1$.

Now, we introduce, for each $T \in \mathcal{T}_h$, the local HHO bilinear form $\hat{a}_T : \underline{\boldsymbol{U}}_T^k \times \underline{\boldsymbol{U}}_T^k \to \mathbb{R}$, such that for any $\underline{\boldsymbol{v}}_T, \underline{\boldsymbol{w}}_T \in \underline{\boldsymbol{U}}_T^k$

$$\hat{a}_T(\underline{\boldsymbol{v}}_T, \underline{\boldsymbol{w}}_T) := (\nabla p_T^{k+1}(\underline{\boldsymbol{v}}_T), \nabla p_T^{k+1}(\underline{\boldsymbol{w}}_T))_T + (\tau_{\partial T} S_{\partial T}^k(\underline{\boldsymbol{v}}_T), S_{\partial T}^k(\underline{\boldsymbol{w}}_T))_{\partial T} + \sum_{F \in \partial T \cap \Gamma_{\mathtt{R}}} (\alpha\, v_F, w_F)_F + \sum_{F \in \partial T \cap \Gamma_{\mathtt{S}}} (v_F, w_F)_F\,.$$

Furthermore, we set the global bilinear form $\hat{a}_h : \underline{\boldsymbol{U}}_h^k \times \underline{\boldsymbol{U}}_h^k \to \mathbb{R}$ as

$$\hat{a}_h(\underline{\boldsymbol{v}}_h, \underline{\boldsymbol{w}}_h) := \sum_{T \in \mathcal{T}_h} \hat{a}_T(\underline{\boldsymbol{v}}_T, \underline{\boldsymbol{w}}_T) \quad \forall\, \underline{\boldsymbol{v}}_h, \underline{\boldsymbol{w}}_h \in \underline{\boldsymbol{U}}_h^k\,.$$

The next result will be useful.

Lemma 3.1 *There exists a positive constant β, independent of h, such that*

$$\hat{a}_h(\underline{\boldsymbol{v}}_h, \underline{\boldsymbol{w}}_h) \le \beta^{-1} ||\underline{\boldsymbol{v}}_h||_h\, ||\underline{\boldsymbol{w}}_h||_h \quad \forall\, \underline{\boldsymbol{v}}_h, \underline{\boldsymbol{w}}_h \in \underline{\boldsymbol{U}}_h^k\,.$$
$$\hat{a}_h(\underline{\boldsymbol{v}}_h, \underline{\boldsymbol{v}}_h) \ge \beta\, ||\underline{\boldsymbol{v}}_h||_h^2 \quad \forall\, \underline{\boldsymbol{v}}_h \in \underline{\boldsymbol{U}}_h^k\,.$$

Proof. It follows similar ideas to the proof of Proposition 2.13 in [25]. We omit further details. □

3.1 HHO scheme for the source problem

Given $g \in L^2(\Gamma_{\mathtt{S}})$, find $\underline{\boldsymbol{u}}_h \in \underline{\boldsymbol{U}}_h^k$ such that $\hat{a}_h(\underline{\boldsymbol{u}}_h, \underline{\boldsymbol{w}}_h) = \sum_{F \in \mathcal{F}_h^{\mathtt{S}}} (g, w_F)_F, \forall\, \underline{\boldsymbol{w}}_h \in \underline{\boldsymbol{U}}_h^k$.

This discrete problem can be written as the following symmetric linear system:

$$\begin{pmatrix} \boldsymbol{A}_{\mathcal{T}\mathcal{T}} & \boldsymbol{A}_{\mathcal{T}\mathcal{F}} \\ \boldsymbol{A}_{\mathcal{F}\mathcal{T}} & \boldsymbol{A}_{\mathcal{F}\mathcal{F}} \end{pmatrix} \begin{pmatrix} \boldsymbol{X}_{\mathcal{T}} \\ \boldsymbol{X}_{\mathcal{F}} \end{pmatrix} = \begin{pmatrix} \boldsymbol{0} \\ \boldsymbol{g}_{\mathcal{F}} \end{pmatrix},$$

where $\boldsymbol{X}_{\mathcal{T}}$ collects the unknowns associated to the mesh cells, while $\boldsymbol{X}_{\mathcal{F}}$ contains the corresponding unknowns to the mesh faces. Since $\boldsymbol{A}_{\mathcal{T}\mathcal{T}}$ results to be block-diagonal and non singular, we can eliminate $\boldsymbol{X}_{\mathcal{T}}$ (Schur's complement), leading to an equivalent linear system in $\boldsymbol{X}_{\mathcal{F}}$, which reads:

$$(\boldsymbol{A}_{\mathcal{F}\mathcal{F}} - \boldsymbol{A}_{\mathcal{F}\mathcal{T}} \boldsymbol{A}_{\mathcal{T}\mathcal{T}}^{-1} \boldsymbol{A}_{\mathcal{T}\mathcal{F}}) \boldsymbol{X}_{\mathcal{F}} = \boldsymbol{g}_{\mathcal{F}}\,.$$

3.2 HHO scheme for the Steklov eigenvalue problem

It reads as: *Find* $(\lambda_h, \underline{\boldsymbol{u}}_h) \in \mathbb{R}^+ \times \underline{\boldsymbol{U}}_h^k$, such that

$$\hat{a}_h(\underline{\boldsymbol{u}}_h, \underline{\boldsymbol{w}}_h) = (\lambda_h + 1) \sum_{F \in \mathcal{F}_h^{\mathtt{S}}} (u_F, w_F)_F \quad \forall\, \underline{\boldsymbol{u}}_h \in \underline{\boldsymbol{U}}_h^k\,. \tag{7}$$

The scheme, in matrix form, can be written as:

$$\begin{pmatrix} \boldsymbol{A}_{\mathcal{T}\mathcal{T}} & \boldsymbol{A}_{\mathcal{T}\mathcal{F}} \\ \boldsymbol{A}_{\mathcal{F}\mathcal{T}} & \boldsymbol{A}_{\mathcal{F}\mathcal{F}} \end{pmatrix} \begin{pmatrix} \boldsymbol{X}_{\mathcal{T}} \\ \boldsymbol{X}_{\mathcal{F}} \end{pmatrix} = (\lambda_h + 1) \begin{pmatrix} \boldsymbol{0} & \boldsymbol{0} \\ \boldsymbol{0} & \boldsymbol{B}_{\mathcal{F}\mathcal{F}} \end{pmatrix} \begin{pmatrix} \boldsymbol{X}_{\mathcal{T}} \\ \boldsymbol{X}_{\mathcal{F}} \end{pmatrix},$$

which, after eliminating $\boldsymbol{X}_{\mathcal{T}}$ as before, we have to solve the generalized eigenvalue problem:

$$(\boldsymbol{A}_{\mathcal{F}\mathcal{F}} - \boldsymbol{A}_{\mathcal{F}\mathcal{T}} \boldsymbol{A}_{\mathcal{T}\mathcal{T}}^{-1} \boldsymbol{A}_{\mathcal{T}\mathcal{F}}) \boldsymbol{X}_{\mathcal{F}} = (\lambda_h + 1)\, \boldsymbol{B}_{\mathcal{F}\mathcal{F}}\, \boldsymbol{X}_{\mathcal{F}}\,.$$

3.3 HHO solver

We consider the cell HHO solver operator $\underline{\hat{\boldsymbol{K}}}_h : L^2(\Gamma_{\mathtt{S}}) \to \underline{\boldsymbol{U}}_h^k$, so that

$$\hat{a}_h(\underline{\hat{\boldsymbol{K}}}_h(g), \underline{\boldsymbol{w}}_h) = \sum_{F \in \mathcal{F}_h^{\mathtt{S}}} (g, w_F)_F \quad \forall\, \underline{\boldsymbol{w}}_h \in \underline{\boldsymbol{U}}_h^k \,. \tag{8}$$

However, since $\underline{\boldsymbol{U}}_h^k$ is not a subspace of $L^2(\Gamma_{\mathtt{S}})$, $\underline{\hat{\boldsymbol{K}}}_h$ is not suitable for the analysis of the approximation of our eigenvalue problem. To overcome this situation, we aim to build a local face HHO solver operator $K_{\mathcal{F}^{\mathtt{S}}} : L^2(\Gamma_{\mathtt{S}}) \to \mathcal{P}_{d-1}^k(\mathcal{F}_h^{\mathtt{S}}) \subseteq L^2(\Gamma_{\mathtt{S}})$. To this end, we adapt the ideas given in [14]. First, we introduce the operator $Z_{\mathcal{T}} : \mathcal{P}_{d-1}^k(\mathcal{F}_h) \to \mathcal{P}_d^k(\mathcal{T}_h)$, so that, for any $v_{\mathcal{F}} \in \mathcal{P}_{d-1}^k(\mathcal{F}_h)$, $Z_{\mathcal{T}}(v_{\mathcal{F}}) \in \mathcal{P}_d^k(\mathcal{T}_h)$ is the unique solution of

$$\hat{a}_h((Z_{\mathcal{T}}(v_{\mathcal{F}}), v_{\mathcal{F}}), (w_h, 0)) = 0 \quad \forall\, w_h \in \mathcal{P}_d^k(\mathcal{T}_h) \,. \tag{9}$$

We also define the operator $Z_{\mathcal{T}}^\dagger : \mathcal{P}_{d-1}^k(\mathcal{F}_h) \to \mathcal{P}_d^k(\mathcal{T}_h)$, so that

$$\hat{a}_h((w_h, 0), (Z_{\mathcal{T}}^\dagger(v_{\mathcal{F}}), v_{\mathcal{F}})) = 0 \quad \forall\, w_h \in \mathcal{P}_d^k(\mathcal{T}_h) \,, \tag{10}$$

We remark that since $\hat{a}_h$ is symmetric, $Z_{\mathcal{T}} = Z_{\mathcal{T}}^\dagger$. Now, we introduce the bilinear form $a_{\mathcal{F}} : \mathcal{P}_{d-1}^k(\mathcal{F}_h) \times \mathcal{P}_{d-1}^k(\mathcal{F}_h) \to \mathbb{R}$, given by

$$a_{\mathcal{F}}(v_{\mathcal{F}}, w_{\mathcal{F}}) := \hat{a}_h((Z_{\mathcal{T}}(v_{\mathcal{F}}), v_{\mathcal{F}}), (Z_{\mathcal{T}}^\dagger(w_{\mathcal{F}}), w_{\mathcal{F}})) \quad \forall\, v_{\mathcal{F}}, w_{\mathcal{F}} \in \mathcal{P}_{d-1}^k(\mathcal{F}_h) \,. \tag{11}$$

Next, we define the solver operator $K_{\mathcal{F}} : L^2(\Gamma_{\mathtt{S}}) \to \mathcal{P}_{d-1}^k(\mathcal{F}_h) \subseteq L^2(\Gamma)$, such that for any $\psi \in L^2(\Gamma_{\mathtt{S}})$, $K_{\mathcal{F}}(\psi) \in \mathcal{P}_{d-1}^k(\mathcal{F}_h)$ is the unique element that satisfies

$$a_{\mathcal{F}}(K_{\mathcal{F}}(\psi), w_{\mathcal{F}}) = (\psi, w_{\mathcal{F}})_{\mathcal{F}_h^{\mathtt{S}}} \quad \forall\, w_{\mathcal{F}} \in \mathcal{P}_{d-1}^k(\mathcal{F}_h) \,. \tag{12}$$

Finally, we set $K_{\mathcal{F}^{\mathtt{S}}} : L^2(\Gamma_{\mathtt{S}}) \to \mathcal{P}_{d-1}^k(\mathcal{F}_h^{\mathtt{S}}) \subseteq L^2(\Gamma_{\mathtt{S}})$, given for each $\psi \in L^2(\Gamma_{\mathtt{S}})$, by $K_{\mathcal{F}^{\mathtt{S}}}(\psi) := K_{\mathcal{F}}(\psi)|_{\Gamma_{\mathtt{S}}}$.

Lemma 3.2 *There holds*

$$\forall\, g \in L^2(\Gamma_{\mathtt{S}}) \,:\, \underline{\hat{\boldsymbol{K}}}_h(g) = \Big((Z_{\mathcal{T}} \circ K_{\mathcal{F}})(g), K_{\mathcal{F}}(g)\Big) \,. \tag{13}$$

Proof. Let $g \in L^2(\Gamma_{\mathtt{S}})$ be fixed. Next, $u_{\mathcal{F}} := K_{\mathcal{F}}(g) \in \mathcal{P}_{d-1}^k(\mathcal{F}_h)$ is such that

$$a_{\mathcal{F}}(u_{\mathcal{F}}, w_{\mathcal{F}}) = (g, w_{\mathcal{F}})_{\mathcal{F}_h^{\mathtt{S}}} \quad \forall\, w_{\mathcal{F}} \in \mathcal{P}_{d-1}^k(\mathcal{F}_h) \,.$$

Now, we set $u_{\mathcal{T}} := (Z_{\mathcal{T}} \circ K_{\mathcal{F}})(g) = Z_{\mathcal{T}}(u_{\mathcal{F}}) \in \mathcal{P}_d^k(\mathcal{T}_h)$. It remains to verify that $\underline{\boldsymbol{u}}_h := (u_{\mathcal{T}}, u_{\mathcal{F}}) \in \underline{\boldsymbol{U}}_h^k$ satisfies the source problem

$$\hat{a}_h(\underline{\boldsymbol{u}}_h, \underline{\boldsymbol{w}}_h) = \sum_{F \in \mathcal{F}_h^{\mathtt{S}}} (g, w_F)_F \quad \forall\, \underline{\boldsymbol{w}}_h \in \underline{\boldsymbol{U}}_h^k \,. \tag{14}$$

Given $\underline{\boldsymbol{w}}_h := (w_{\mathcal{T}}, w_{\mathcal{F}}) \in \underline{\boldsymbol{U}}_h^k$ fixed, we decompose it as $\underline{\boldsymbol{w}}_h = \underline{\boldsymbol{x}}_h + \underline{\boldsymbol{y}}_h$, where $\underline{\boldsymbol{x}}_h := (0_{\mathcal{T}}, w_{\mathcal{F}}) \in \underline{\boldsymbol{U}}_h^k$ and $\underline{\boldsymbol{y}}_h := (w_{\mathcal{T}}, 0_{\mathcal{F}}) \in \underline{\boldsymbol{U}}_h^k$. Now, taking $\underline{\boldsymbol{x}}_h$, we have

$$\begin{aligned}
\hat{a}_h(\underline{\boldsymbol{u}}_h, \underline{\boldsymbol{x}}_h) &= \hat{a}_h((u_{\mathcal{T}}, u_{\mathcal{F}})(0, w_{\mathcal{F}})) \\
&= \hat{a}_h((Z_{\mathcal{T}}(u_{\mathcal{F}}), u_{\mathcal{F}})(0, w_{\mathcal{F}})) + \underbrace{\hat{a}_h((Z_{\mathcal{T}}(u_{\mathcal{F}}), u_{\mathcal{F}}), (Z_{\mathcal{T}}^\dagger(w_{\mathcal{F}}), 0))}_{=0} \\
&= \hat{a}_h((Z_{\mathcal{T}}(u_{\mathcal{F}}), u_{\mathcal{F}}), (Z_{\mathcal{T}}^\dagger(w_{\mathcal{F}}), w_{\mathcal{F}})) \\
&= a_{\mathcal{F}}(u_{\mathcal{F}}, w_{\mathcal{F}}) = (g, w_{\mathcal{F}})_{\mathcal{F}_h^{\mathtt{S}}} \,.
\end{aligned}$$

On the other hand, and taking into account (9), we have

$$\hat{a}_h(\underline{\boldsymbol{u}}_h, \underline{\boldsymbol{y}}_h) = \hat{a}_h((u_{\mathcal{T}}, u_{\mathcal{F}}), (w_{\mathcal{T}}, 0_{\mathcal{F}})) = 0\,,$$

and we conclude that $\hat{a}_h(\underline{\boldsymbol{u}}_h, \underline{\boldsymbol{w}}_h) = (g, w_{\mathcal{F}})_{\mathcal{F}_h^{\mathtt{s}}}$, $\forall\, \underline{\boldsymbol{w}}_h \in \underline{\boldsymbol{U}}_h^k$. Finally, (13) has been established, by the uniqueness of the solution, and we end the proof. □

Remark 3.1 *We notice that $(\lambda_h + 1, \underline{\boldsymbol{u}}_h) \in \mathbb{R}^+ \times \underline{\boldsymbol{U}}_h^k$, with $\underline{\boldsymbol{u}}_h := (u_{\mathcal{T}}, u_{\mathcal{F}})$, is an eigenpair of* (7) *if and only if $u_{\mathcal{T}} = Z_{\mathcal{T}}(u_{\mathcal{F}})$, and $(\lambda_h, u_{\mathcal{F}}) \in \mathbb{R}^+ \times \mathcal{P}_{d-1}^k(\mathcal{F})$ verifies*

$$a_{\mathcal{F}}(u_{\mathcal{F}}, w_{\mathcal{F}}) = (\lambda_h + 1)\,(u_{\mathcal{F}}, w_{\mathcal{F}})_{\mathcal{F}_h^{\mathtt{s}}} \quad \forall\, w_{\mathcal{F}} \in \mathcal{P}_{d-1}^k(\mathcal{F})\,. \tag{15}$$

This is equivalent to say that $(\mu_h, u_{\mathcal{F}}) \in \mathbb{R}^+ \times \mathcal{P}_{d-1}^k(\mathcal{F})$, with $\mu_h = \frac{1}{\lambda_h+1}$, is an eigenpair of the discrete solver $K_{\mathcal{F}}$.

Lemma 3.3 *The operator $K_{\mathcal{F}^{\mathtt{s}}} : L^2(\Gamma_{\mathtt{s}}) \to \mathcal{P}_{d-1}^k(\mathcal{F}_h^{\mathtt{s}}) \subseteq L^2(\Gamma_{\mathtt{s}})$, is self-adjoint and positive. Moreover, if $(\lambda_h, u_{\mathcal{F}}) \in \mathbb{R}^+ \times \mathcal{P}_{d-1}^k(\mathcal{F})$ satisfies* (15)*, then $\left(\frac{1}{\lambda_h+1}, u_{\mathcal{F}}|_{\mathcal{F}^{\mathtt{s}}}\right)$ is an eigenpair of $K_{\mathcal{F}^{\mathtt{s}}}$.*

Proof. *We first let $\psi, \varphi \in L^2(\Gamma_{\mathtt{s}})$ be fixed. Then, there holds*

$$a_{\mathcal{F}}(K_{\mathcal{F}}(\psi), w_{\mathcal{F}}) = (\psi, w_{\mathcal{F}})_{\mathcal{F}_h^{\mathtt{s}}} \quad \forall\, w_{\mathcal{F}} \in \mathcal{P}_{d-1}^k(\mathcal{F})\,. \tag{16}$$

$$a_{\mathcal{F}}(K_{\mathcal{F}}(\varphi), v_{\mathcal{F}}) = (\varphi, v_{\mathcal{F}})_{\mathcal{F}_h^{\mathtt{s}}} \quad \forall\, v_{\mathcal{F}} \in \mathcal{P}_{d-1}^k(\mathcal{F})\,. \tag{17}$$

Now, choosing $w_{\mathcal{F}} := K_{\mathcal{F}}(\varphi)$ and $v_{\mathcal{F}} := K_{\mathcal{F}}(\psi)$, and taking into account the symmetry of $a_{\mathcal{F}}$, we deduce

$$(\psi, K_{\mathcal{F}^{\mathtt{s}}}(\varphi))_{\mathcal{F}_h^{\mathtt{s}}} = (\psi, K_{\mathcal{F}}(\varphi))_{\mathcal{F}_h^{\mathtt{s}}} = (\varphi, K_{\mathcal{F}}(\psi))_{\mathcal{F}_h^{\mathtt{s}}} = (\varphi, K_{\mathcal{F}^{\mathtt{s}}}(\psi))_{\mathcal{F}_h^{\mathtt{s}}} = (K_{\mathcal{F}^{\mathtt{s}}}(\psi), \varphi)_{\mathcal{F}_h^{\mathtt{s}}}\,.$$

The latter ensures that $K_{\mathcal{F}^{\mathtt{s}}}$ is self-adjoint. On the other hand, taking $w_{\mathcal{F}} := K_{\mathcal{F}}(\psi)$ in (16)*, results*

$$(\psi, K_{\mathcal{F}^{\mathtt{s}}}(\psi))_{\mathcal{F}_h^{\mathtt{s}}} = (\psi, K_{\mathcal{F}}(\psi))_{\mathcal{F}_h^{\mathtt{s}}} = a_{\mathcal{F}}(K_{\mathcal{F}}(\psi), K_{\mathcal{F}}(\psi))\,.$$

Then, recalling that $a_{\mathcal{F}}$ is symmetric and elliptic, we infer that $K_{\mathcal{F}^0}$ is positive.

Next, we consider $(\lambda_h, u_{\mathcal{F}}) \in \mathbb{R}^+ \times \mathcal{P}_{d-1}^k(\mathcal{F})$, that satisfies (15)*, and set $K_{\mathcal{F}^{\mathtt{s}}}(u_{\mathcal{F}}|_{\mathcal{F}^{\mathtt{s}}}) = z_{\mathcal{F}}|_{\Gamma_{\mathtt{s}}}$, with $z_{\mathcal{F}} := K_{\mathcal{F}}(u_{\mathcal{F}})$. Then*

$$a_{\mathcal{F}}(z_{\mathcal{F}}, w_{\mathcal{F}}) = (u_{\mathcal{F}}, w_{\mathcal{F}})_{\mathcal{F}_h^{\mathtt{s}}} \quad \forall\, w_{\mathcal{F}} \in \mathcal{P}_{d-1}^k(\mathcal{F})\,. \tag{18}$$

Comparing (18) *and* (15)*, we obtain*

$$u_{\mathcal{F}} = (\lambda_h + 1) z_{\mathcal{F}} \quad \Rightarrow \quad K_{\mathcal{F}^{\mathtt{s}}}(u_{\mathcal{F}}|_{\mathcal{F}^{\mathtt{s}}}) = \frac{1}{\lambda_h + 1} u_{\mathcal{F}}|_{\mathcal{F}^{\mathtt{s}}}\,.$$

□

Lemma 3.4 *There exists $C > 0$, independent of h, such that*

$$\forall\, g \in L^2(\Gamma_{\mathtt{s}}) \,:\, ||\hat{\underline{\boldsymbol{K}}}_h(g)||_h \,\leq\, C\,||g||_{0,\Gamma_{\mathtt{s}}}\,. \tag{19}$$

Proof. Let $g \in L^2(\Gamma_{\mathtt{S}})$ be fixed, and set $\underline{\hat{\boldsymbol{K}}}_h(g) := \underline{\boldsymbol{u}}_h = (u_{\mathcal{T}}, u_{\mathcal{F}}) \in \underline{\boldsymbol{U}}_h^k$, such that $\hat{a}_h(\underline{\hat{\boldsymbol{K}}}_h(g), \underline{\boldsymbol{v}}_h) = (g, v_{\mathcal{F}})_{\mathcal{F}_h^{\mathtt{S}}}$, for all $\underline{\boldsymbol{v}}_h = (v_{\mathcal{T}}, v_{\mathcal{F}}) \in \underline{\boldsymbol{U}}_h^k$. Then, we have

$$\beta \, ||\underline{\hat{\boldsymbol{K}}}_h(g)||_h^2 \, \leq \hat{a}_h(\underline{\hat{\boldsymbol{K}}}_h(g), \underline{\hat{\boldsymbol{K}}}_h(g)) = (g, u_{\mathcal{F}})_{\mathcal{F}_h^{\mathtt{S}}} \leq ||g||_{0,\Gamma_{\mathtt{S}}} \, ||u_{\mathcal{F}}||_{0,\Gamma_{\mathtt{S}}} \, .$$

On the other hand,

$$||u_{\mathcal{F}}||_{0,\Gamma_{\mathtt{S}}} \leq ||u_{\mathcal{F}}||_{0,\Gamma_h} = ||\gamma_h(\underline{\boldsymbol{u}}_h)||_{0,\Gamma} \leq C_{\mathtt{tr}} \, ||\underline{\boldsymbol{u}}_h||_h \, .$$

after invoking a well known HHO trace inequality (we refer to Lemma 5.1 in the Appendix). Finally, we end the proof. □

REGULARITY ASSUMPTION: In what follows, we assume that given $g \in L^2(\Gamma_{\mathtt{S}})$, the solution $u(g)$ of the source problem (4) that defines g, belongs to $H^{1+t}(\Omega)$, for some $t \in (0, t_0)$. In addition, there exists $C > 0$, independent of h, such that $||u(g)||_{1+t,\Omega} \leq C \, ||g||_{0,\Gamma_{\mathtt{S}}}$.

This holds, for example, for a polygonal domain $\Omega \subseteq \mathbb{R}^2$ (cf. Corollary 3.1 in [33]). We also remark that $t_0 = 1/2$ when $\Gamma_{\mathtt{S}} = \Gamma$ or $\Gamma_{\mathtt{R}} = \emptyset$ (cf. Theorem 4 in [39]).

Lemma 3.5 *There exists $C > 0$, independent of h, such that*

$$||\underline{\hat{\boldsymbol{K}}}_h(g) - \underline{\hat{\boldsymbol{I}}}_h^k(u)||_h \, \leq \, C \, h^s \, ||K(g)||_{1/2+s,\Gamma_{\mathtt{S}}} \, , \tag{20}$$

for all $s \in [t, k+1]$, and all $g \in L^2(\Gamma_{\mathtt{S}})$ such that $u \in H^{1+s}(\Omega)$, with u satisfying $K(g) = \gamma(u)|_{\Gamma_{\mathtt{S}}}$. Here, t is the corresponding smoothness index from the elliptic regularity theory.

Proof. We invoke the Third Strang's Lemma (cf. Lemma A.7 in [25]), to obtain

$$||\underline{\hat{\boldsymbol{K}}}_h(g) - \underline{\hat{\boldsymbol{I}}}_h^k(u)||_h \, \leq \, C \quad \sup_{\substack{\underline{\boldsymbol{w}}_h \in \underline{\boldsymbol{U}}_h^k \\ ||\underline{\boldsymbol{w}}_h||_h = 1}} |\mathcal{E}_h(u; \underline{\boldsymbol{w}}_h)| \, ,$$

where the consistency term $\mathcal{E}_h(u; \cdot)$ is defined as

$$\mathcal{E}_h(u; \underline{\boldsymbol{w}}_h) := \hat{a}_h(\underline{\hat{\boldsymbol{I}}}_h^k(u), \underline{\boldsymbol{w}}_h) - (g, w_{\mathcal{F}})_{\mathcal{F}_h^{\mathtt{S}}} \quad \forall \, \underline{\boldsymbol{w}}_h \in \underline{\boldsymbol{U}}_h^k \, .$$

It is known that

$$\begin{aligned} \mathcal{E}_h(u; \underline{\boldsymbol{w}}_h) = & \sum_{T \in \mathcal{T}_h} \Big(\nabla p_T^{k+1} \underline{\boldsymbol{I}}_T^k(u) - \nabla u, \nabla w_T \Big)_T + \sum_{F \in \mathcal{F}_T} (\nabla p_T^{k+1} \underline{\boldsymbol{I}}_T^k(u) \cdot \boldsymbol{n} - \nabla u \cdot \boldsymbol{n}, w_F - w_T)_F \\ & + s_h(\underline{\boldsymbol{I}}_T^k(u), \underline{\boldsymbol{w}}_h) \, . \end{aligned}$$

Finally, the result is obtained after applying suitable Cauchy-Schwarz, and the approximation properties of $p_T^{k+1} \underline{\boldsymbol{I}}_T^k$, $\underline{\boldsymbol{I}}_T^k$ and s_h. We omit further details. □

4 A priori error analysis

We set $\mathrm{L} := L^2(\Gamma_{\mathtt{S}})$.

Lemma 4.1 *There exists $C > 0$, independent of h, such that*

$$\sup_{(\psi,\varphi) \in \mathrm{L} \times \mathrm{L}} |((K - K_{\mathcal{F}^{\mathtt{S}}})(\psi), \varphi)_{\mathrm{L}}| \leq C \, h^{\min\{k+1, t+1/2\}} \, ||\psi||_{\mathrm{L}} \, ||\varphi||_{\mathrm{L}} \, , \tag{21}$$

with t being the corresponding smoothness index from the elliptic regularity theory. As a consequence, we have $||K - K_{\mathcal{F}^{\mathtt{S}}}||_{\mathcal{L}(\mathrm{L})}$, as h goes to 0.

Proof. First, we let $\psi, \varphi \in \mathrm{L}$ be fixed. Denoting by u the exact solution of source problem (4) with $g := \psi$, and recalling that $K(\psi) = u$ on $\Gamma_{\mathtt{S}}$ and $\hat{a}_h$ is symmetric, we notice that

$$\hat{a}_h(\hat{\underline{\boldsymbol{I}}}_h^k(u), \hat{\underline{\boldsymbol{K}}}_h(\varphi)) = \hat{a}_h(\hat{\underline{\boldsymbol{K}}}_h(\varphi), \hat{\underline{\boldsymbol{I}}}_h^k(u)) = (\varphi, \pi^k_{\mathcal{F}_h} u)_{\mathrm{L}} = (\pi^k_{\mathcal{F}_h}(K(\psi)), \varphi)_{\mathrm{L}}\,.$$

Then, we derive

$$\begin{aligned}
((K - K_{\mathcal{F}^{\mathtt{S}}})(\psi), \varphi)_{\mathrm{L}} &= (K(\psi), \varphi)_{\mathrm{L}} - (K_{\mathcal{F}^0}(\psi), \varphi)_{\mathrm{L}} = (K(\psi), \varphi)_{\mathrm{L}} - (\varphi, K_{\mathcal{F}}(\psi))_{\mathrm{L}} \\
&= (K(\psi), \varphi)_{\mathrm{L}} - a_{\mathcal{F}}(K_{\mathcal{F}}(\varphi), K_{\mathcal{F}}(\psi)) \\
&= (K(\psi), \varphi)_{\mathrm{L}} - a_{\mathcal{F}}(K_{\mathcal{F}}(\psi), K_{\mathcal{F}}(\varphi)) \\
&= (K(\psi), \varphi)_{\mathrm{L}} - \hat{a}_h(\hat{\underline{\boldsymbol{K}}}_h(\psi), \hat{\underline{\boldsymbol{K}}}_h(\varphi)) \\
&= (K(\psi), \varphi)_{\mathrm{L}} - \hat{a}_h(\hat{\underline{\boldsymbol{I}}}_h^k(u), \hat{\underline{\boldsymbol{K}}}_h(\varphi)) + \hat{a}_h(\hat{\underline{\boldsymbol{I}}}_h^k(u) - \hat{\underline{\boldsymbol{K}}}_h(\psi), \hat{\underline{\boldsymbol{K}}}_h(\varphi)) \\
&= \underbrace{(K(\psi) - \pi^k_{\mathcal{F}_h}(K(\psi)), \varphi)_{\mathrm{L}}}_{=:\mathfrak{I}_1} + \underbrace{\hat{a}_h(\hat{\underline{\boldsymbol{I}}}_h^k(u) - \hat{\underline{\boldsymbol{K}}}_h(\psi), \hat{\underline{\boldsymbol{K}}}_h(\varphi))}_{=:\mathfrak{I}_2}\,. \qquad (22)
\end{aligned}$$

Next, we proceed to bound $\mathfrak{I}_1$ and $\mathfrak{I}_2$.

BOUNDING $\mathfrak{I}_1$: First, we let $F \in \mathcal{F}_h^{\mathtt{S}}$ be fixed, and set $T_F \in \mathcal{T}_h$ such that F is one its faces. We notice that

$$u - \pi^k_F u = (u - \pi^k_{T_F} u) - \pi^k_F(u - \pi^k_{T_F} u)\,.$$

Next, by applying Cauchy-Schwarz inequality and invoking standard approximation properties, we get

$$|\mathfrak{I}_1| \,\leq\, ||K(\psi) - \pi^k_{\mathcal{F}_h}(K(\psi)||_{\mathrm{L}}\, ||\varphi||_{\mathrm{L}} \,\leq\, C\, h^{1/2}\, ||\psi||_{\mathrm{L}}\, ||\varphi||_{\mathrm{L}}\,.$$

BOUNDING $\mathfrak{I}_2$: Invoking the boundedness of $\hat{a}_h$ (cf. Lemma 3.1), we obtain

$$|\mathfrak{I}_2| \,\leq \beta^{-1}\, ||\hat{\underline{\boldsymbol{I}}}_h^k(u) - \hat{\underline{\boldsymbol{K}}}_h(\psi)||_h\, ||\hat{\underline{\boldsymbol{K}}}_h(\varphi)||_h\,.$$

Now, thanks to Lemmas 3.5 and 3.4, as well as the REGULARITY ASSUMPTION, we derive

$$|\mathfrak{I}_2| \,\leq \beta^{-1}\, \tilde{C}\, h^{\min\{k+1, t+1/2\}}\, ||\psi||_{\mathrm{L}}\, ||\varphi||_{\mathrm{L}}\,.$$

Finally, using these bounds for $\mathfrak{I}_1$ and $\mathfrak{I}_2$, we conclude the proof. □

In what follows we give a description of the main results on the spectral approximation of compact operators in Hilbert spaces. Let $\sigma(K)$ be the spectrum of the compact operator K, and let $\mu \in \sigma(K)\backslash\{0\}$ be a nonzero eigenvalue of K. Let $\beta \in \mathbb{Z}^+$ be the ascent of μ, i.e., the smallest positive integer β such that $\mathrm{Ker}(\mu\, I - K)^\beta = \mathrm{Ker}(\mu\, I - K)^{\beta+1}$, where I denotes the identity operator. We also define

$$G_\mu := \mathrm{Ker}(\mu\, I - K)^\beta\,, \quad G^*_\mu := \mathrm{Ker}(\mu\, I - K^*)^\beta\,,$$

and $m := \dim(G_\mu)$, which is known as the algebraic multiplicity of μ. We recall that $m \geq \beta$. Now, we assume that there exist $s \in [t, k+1]$ and $C_s > 0$, such that

$$\forall\, \psi \in G_\mu \,:\, ||\psi||_{1/2+s,\Gamma_{\mathtt{S}}} + ||u(\psi)||_{1+s,\Omega} \leq C_s\, ||\psi||_{\mathrm{L}}\,, \qquad (23)$$

$$\forall\, \varphi \in G^*_\mu \,:\, ||\varphi||_{1/2+s,\Gamma_{\mathtt{S}}} + ||u(\varphi)||_{1+s,\Omega} \leq C_s\, ||\varphi||_{\mathrm{L}}\,. \qquad (24)$$

Remark 4.1 *If $s = t$, functions in G_μ and G_μ^* do not provide additional smoothness with respect to that resulting from the elliptic regularity theory. It is known that usually, functions in G_μ and G_μ^* are smoother, and one has $s > t$. The case $s = k + 1$ leads to optimar error estimates.*

Next result gives us useful bounds.

Lemma 4.2 *There exists $C > 0$, independent of h, such that*

$$\sup_{(\psi,\varphi)\in G_\mu\times \mathrm{L}} |((K - K_{\mathcal{F}^{\mathrm{s}}})(\psi), \varphi)_{\mathrm{L}}| \leq C\, h^s\, ||\psi||_{\mathrm{L}}\, ||\varphi||_{\mathrm{L}}\,, \tag{25}$$

with $s \in [t, k + 1]$ being the smoothness index corresponding to the elements in G_μ. As a consequence, we have

$$||(K - K_{\mathcal{F}^{\mathrm{s}}})|_{G_\mu}||_{\mathcal{L}(G_\mu,\mathrm{L})} \;\leq\; C\, h^s\,. \tag{26}$$

Proof. We let $(\psi, \varphi) \in G_\mu \times \mathrm{L}$ be fixed. As before, our aim is to bound each term on the right hand side in (22). Taking into account (23), we deduce

$$|\mathfrak{I}_1| \leq C\, h^{\min\{k+1,s+1/2\}} ||u(\psi)||_{1+s,\Omega}\, ||\varphi||_{\mathrm{L}} \leq C\, C_s\, h^{\min\{k+1,s+1/2\}}\, ||\psi||_{\mathrm{L}}\, ||\varphi||_{\mathrm{L}}\,.$$

Similarly, we obtain, after invoking Lemma 3.4

$$|\mathfrak{I}_2| \;\leq\; \beta^{-1}\, \tilde{C}\, C_s\, h^{\min\{k+1,s+1/2\}}\, ||\psi||_{\mathrm{L}}\, ||\varphi||_{\mathrm{L}}\,.$$

We omit further details. □

Lemma 4.3 *There exists $C > 0$, independent of h, such that*

$$\sup_{(\psi,\varphi)\in G_\mu\times G_\mu^*} |((K - K_{\mathcal{F}^{\mathrm{s}}})(\psi), \varphi)_{\mathrm{L}}| \leq C\, h^{2s}\, ||\psi||_{\mathrm{L}}\, ||\varphi||_{\mathrm{L}}\,, \tag{27}$$

with $s \in [t, k + 1]$ being the smoothness index corresponding to the elements of G_μ and G_μ^*.

Proof. We let $(\psi, \varphi) \in G_\mu \times G_\mu^*$ be fixed. The starting point is the identity (22). In this case, we can take advantage of the smoothness of both ψ and φ, to find sharper bounds of $\mathfrak{I}_1$ and $\mathfrak{I}_2$. In the case of $\mathfrak{I}_1$, we notice that

$$\begin{aligned} &\mathfrak{I}_1 = (K(\psi) - \pi^k_{\mathcal{F}_h}(K(\psi)), \varphi)_{\mathrm{L}} = (K(\psi) - \pi^k_{\mathcal{F}_h}(K(\psi)), \varphi - \pi^k_{\mathcal{F}_h}(\varphi))_{\mathrm{L}} \\ \Rightarrow\; &|\mathfrak{I}_1| \leq C\, h^{2\min\{k+1,s+1/2\}} ||K(\psi)||_{s+1/2,\Gamma_{\mathrm{s}}}\, ||\varphi||_{s+1/2,\Gamma_{\mathrm{s}}} \leq C\, C_s^2\, h^{2\min\{k+1,s+1/2\}} ||\psi||_{\mathrm{L}}\, ||\varphi||_{\mathrm{L}}\,, \end{aligned}$$

after invoking (23).

Next, we bound $\mathfrak{I}_2$, considering the smoothness of both ψ and φ, too. To this end, we have

$$\begin{aligned} \mathfrak{I}_2 \;&= \hat{a}_h(\underline{\hat{\boldsymbol{I}}}^k_h(u) - \underline{\hat{\boldsymbol{K}}}_h(\psi), \underline{\hat{\boldsymbol{K}}}_h(\varphi)) \\ &= \hat{a}_h(\underline{\hat{\boldsymbol{I}}}^k_h(u(\psi)) - \underline{\hat{\boldsymbol{K}}}_h(\psi), \underline{\hat{\boldsymbol{I}}}^k_h(u(\varphi))) + \hat{a}_h(\underline{\hat{\boldsymbol{I}}}^k_h(u) - \underline{\hat{\boldsymbol{K}}}_h(\psi), \underline{\hat{\boldsymbol{K}}}_h(\varphi) - \underline{\hat{\boldsymbol{I}}}^k_h(u(\varphi))) \\ &= \hat{a}_h(\underline{\hat{\boldsymbol{I}}}^k_h(u(\psi)), \underline{\hat{\boldsymbol{I}}}^k_h(u(\varphi))) - \hat{a}_h(\underline{\hat{\boldsymbol{K}}}_h(\psi), \underline{\hat{\boldsymbol{I}}}^k_h(u(\varphi))) + \hat{a}_h(\underline{\hat{\boldsymbol{I}}}^k_h(u) - \underline{\hat{\boldsymbol{K}}}_h(\psi), \underline{\hat{\boldsymbol{K}}}_h(\varphi) - \underline{\hat{\boldsymbol{I}}}^k_h(u(\varphi)))\,. \end{aligned}$$

We notice that

$$\begin{aligned} -\hat{a}_h(\underline{\hat{\boldsymbol{K}}}_h(\psi), \underline{\hat{\boldsymbol{I}}}^k_h(u(\varphi))) \;&=\; -(\psi, \pi^k_{\mathcal{F}^0_h}(u(\varphi)))_{\mathrm{L}} = (\psi, u(\varphi) - \pi^k_{\mathcal{F}^0_h}(u(\varphi)))_{\mathrm{L}} - (\psi, u(\varphi))_{\mathrm{L}} \\ &= (\psi - \pi^k_{\mathcal{F}^0_h}(\psi), u(\varphi) - \pi^k_{\mathcal{F}^0_h}(u(\varphi)))_{\mathrm{L}} - a(u(\psi), u(\varphi))\,, \end{aligned}$$

which allows us to establish

$$\begin{aligned}\mathfrak{I}_2 \,&=\, (\psi-\pi^k_{\mathcal{F}^0_h}(\psi),u(\varphi)-\pi^k_{\mathcal{F}^0_h}(u(\varphi)))_{\mathrm{L}}\\ &\quad+\,\hat{a}_h(\hat{\underline{\boldsymbol{I}}}^k_h(u(\psi)),\hat{\underline{\boldsymbol{I}}}^k_h(u(\varphi)))-a(u(\psi),u(\varphi))\\ &\quad+\,\hat{a}_h(\hat{\underline{\boldsymbol{I}}}^k_h(u(\psi))-\hat{\underline{\boldsymbol{K}}}_h(\psi),\hat{\underline{\boldsymbol{K}}}_h(\varphi)-\hat{\underline{\boldsymbol{I}}}^k_h(u(\varphi)))\\ &=\,\mathfrak{I}_{2,1}+\mathfrak{I}_{2,2}+\mathfrak{I}_{2,3}\,.\end{aligned}$$

Now, we bound each of the three summands referred above. First, we invoke approximation theory, (23) and (24), to obtain

$$|\mathfrak{I}_{2,1}|\leq C\,C_t^2\,h^{2\min\{k+1,s+1/2\}}\,||\psi||_{\mathrm{L}}\,||\varphi||_{\mathrm{L}}\,.$$

Next, to bound $\mathfrak{I}_{2,3}$, we take into account the boundedness of $\hat{a}_h$, and apply Lemma 3.4. As a result, we derive

$$|\mathfrak{I}_{2,3}|\leq C\,h^{2\min\{k+1,s+1/2\}}\,||K(\psi)||_{s+1/2,\Gamma_{\mathrm{s}}}\,||K(\varphi)||_{s+1/2,\Gamma_{\mathrm{s}}}\leq C\,C_s^2\,h^{2\min\{k+1,s+1/2\}}\,||\psi||_{\mathrm{L}}\,||\varphi||_{\mathrm{L}}\,.$$

It is the turn of bounding $\mathfrak{I}_{2,2}$. We notice that

$$\begin{aligned}\mathfrak{I}_{2,2}\,&=\,\sum_{T\in\mathcal{T}_h}(\nabla p_T^{k+1}\hat{\underline{\boldsymbol{I}}}^k_T(u(\psi))),\nabla p_T^{k+1}\hat{\underline{\boldsymbol{I}}}^k_T(u(\varphi)))_T-(\nabla u(\psi),\nabla u(\varphi))_T\\ &\quad+\,s_h(\hat{\underline{\boldsymbol{I}}}^k_h(u(\psi)),\hat{\underline{\boldsymbol{I}}}^k_h(u(\varphi)))\\ &\quad+\,\sum_{F\in\mathcal{F}_h^{\mathrm{R}}}\alpha\,(\pi^k_F(u(\psi))-u(\psi),u(\varphi)-\pi^k_F(u(\varphi)))_F\\ &\quad+\,\sum_{F\in\mathcal{F}_h^{\mathrm{S}}}(\pi^k_F(u(\psi))-u(\psi),u(\varphi)-\pi^k_F(u(\varphi)))_F\\ &=\,\mathfrak{I}_{2,2,1}+\mathfrak{I}_{2,2,2}+\mathfrak{I}_{2,2,3}+\mathfrak{I}_{2,2,4}\,.\end{aligned}$$

At this point, we take advantage that $\nabla p_T^{k+1}\hat{\underline{\boldsymbol{I}}}^k_T$ corresponds to the elliptic projector. Then we have

$$\mathfrak{I}_{2,2,1}\,=\,-\sum_{T\in\mathcal{T}_h}(\nabla(u(\psi)-p_T^{k+1}\hat{\underline{\boldsymbol{I}}}^k_T(u(\varphi)),\nabla(u(\psi)-p_T^{k+1}\hat{\underline{\boldsymbol{I}}}^k_T(u(\varphi))))_T\,.$$

Invoking Cauchy-Schwarz inequality and the approximation properties of the elliptic projector, we deduce that

$$|\mathfrak{I}_{2,2,1}|\leq C\,h^{2s}\,||u(\psi)||_{s+1/2,\Gamma_{\mathrm{s}}}\,||u(\varphi)||_{s+1/2,\Gamma_{\mathrm{s}}}\leq C\,C_s^2\,h^{2s}\,||\psi||_{\mathrm{L}}\,||\varphi||_{\mathrm{L}}\,.$$

On the other hand, applying the consistency property of s_h, we obtain

$$|\mathfrak{I}_{2,2,2}|\leq s_h^{1/2}(\hat{\underline{\boldsymbol{I}}}^k_h(u(\psi)),\hat{\underline{\boldsymbol{I}}}^k_h(u(\psi)))\,s_h^{1/2}(\hat{\underline{\boldsymbol{I}}}^k_h(u(\varphi)),\hat{\underline{\boldsymbol{I}}}^k_h(u(\varphi)))\leq C\,C_s^2\,h^{2s}\,||\psi||_{\mathrm{L}}\,||\varphi||_{\mathrm{L}}\,.$$

To bound $\mathfrak{I}_{2,2,3}$ and $\mathfrak{I}_{2,2,4}$, we apply Cauchy-Schwarz inequality and the approximation properties of L^2 orthogonal projector, to establish

$$\begin{aligned}|\mathfrak{I}_{2,2,3}|&\leq\alpha\,C\,C_s^2\,h^{2s}\,||\psi||_{\mathrm{L}}\,||\varphi||_{\mathrm{L}}\,,\\ |\mathfrak{I}_{2,2,4}|&\leq C\,C_s^2\,h^{2s}\,||\psi||_{\mathrm{L}}\,||\varphi||_{\mathrm{L}}\,.\end{aligned}$$

Finally, we collect the above estimates and conclude the proof. □

Now, we are in position to establish the main results of the current work. To this aim, we let $\mu \in \sigma(K)\backslash\{0\}$ with ascent ϵ and algebraic multiplicity m. Since K is a self-adjoint operator, we have $\epsilon = 1$. Thanks to the convergence result from Lemma 4.1, $K_{\mathcal{F}^0}$ admits m eigenvalues $\{\mu_{h,j}\}_{j=1}^m$, so that each one of them converges to μ as $h \to 0$.

Theorem 4.1 (Error estimate on eigenvalues and eigenfunctions in L**)** *Assume that there is $s \in [t, k+1]$ so that there hold the smoothness properties* (23) *and* (24)*, where $t > 0$ is the smoothnes index resulting from the elliptic regularity theory. Then there is $C > 0$, independent of h, but depending on μ, the mesh regularity, the polynomial degree k and the domain Ω, such that*

$$\max_{1\leq j\leq m} |\mu - \mu_{h,j}| + |\mu - \widehat{\mu}_h| \leq C\, h^{2s}\,, \tag{28}$$

where $\widehat{\mu}_h := \dfrac{1}{m}\displaystyle\sum_{j=1}^{m} \mu_{h,j}$ is the very well known arithmetic mean. Moreover, let $v_{\mathcal{F},j} \in \mathcal{P}_{d-1}^k(\mathcal{F}_h^{\mathtt{S}})$ be a unit vector belonging to $\mathrm{Ker}(\mu_{h,j} I - K_{\mathcal{F}^{\mathtt{S}}})$. Then, there is a unit vector $v_j \in \mathrm{Ker}(\mu\, I - K) \subseteq G_\mu$, such that

$$||v_j - v_{\mathcal{F},j}||_{\mathrm{L}} \leq C\, h^s\,. \tag{29}$$

Proof. (28) is a straightforward consequence of Lemmas 4.2, 4.3, with Theorems 7.2 and 7.3 in [8]. Similarly, invoking Theorem 7.4 in [8] and taking into consideration Lemma 4.2, we conclude (29). □

Remark 4.2 *Since the eigenvalues λ and λ_h associated to* (3) *and* (7)*, respectively, are such that $\lambda = \mu^{-1} - 1$ and $\lambda_h = \mu_h^{-1} - 1$, we infer that the same estimate as* (28) *holds true for the error between λ and λ_h.*

Corollary 4.1 *Under the same assumptions and notations as considered in Theorem 4.1, but dropping the index j from the eigenfunction v_j and the approximate eigenfunction $v_{\mathcal{F},j}$. Then, setting $\underline{\boldsymbol{v}}_h := (Z_{\mathcal{T}}(v_{\mathcal{F}}), v_{\mathcal{F}}) \in \underline{\boldsymbol{U}}_h^k$, there exists $C > 0$, independent of the mesh size, such that*

$$\hat{a}_h(\underline{\boldsymbol{v}}_h - \underline{\hat{\boldsymbol{I}}}_h^k(v), \underline{\boldsymbol{v}}_h - \underline{\hat{\boldsymbol{I}}}_h^k(v)) \leq C\, h^{2s}\,. \tag{30}$$

As a consequence, we have

$$||\nabla(v - p_h^{k+1}(\underline{\boldsymbol{v}}_h))||_{0,\Omega}^2 \leq C\, h^{2s}\,. \tag{31}$$

Proof. We notice that

$$\begin{aligned}
(\lambda_h + 1)(v_{\mathcal{F}}, v)_{\mathrm{L}} &= (\lambda_h + 1)(v_{\mathcal{F}}, \pi_{\mathcal{F}}^k(v))_{\mathrm{L}} = a_{\mathcal{F}}(v_{\mathcal{F}}, \pi_{\mathcal{F}}^k(v)) \\
&= \hat{a}_h((Z_{\mathcal{T}}(v_{\mathcal{F}}), v_{\mathcal{F}}), (Z_{\mathcal{T}}^\dagger(\pi_{\mathcal{F}}^k(v)), \pi_{\mathcal{F}}^k(v))) \\
&= \hat{a}_h((Z_{\mathcal{T}}(v_{\mathcal{F}}), v_{\mathcal{F}}), (Z_{\mathcal{T}}^\dagger(\pi_{\mathcal{F}}^k(v)), \pi_{\mathcal{F}}^k(v))) \\
&\quad + \underbrace{\hat{a}_h((Z_{\mathcal{T}}(v_{\mathcal{F}}), v_{\mathcal{F}}), (\pi_{\mathcal{T}}^k(v) - Z_{\mathcal{T}}^\dagger(\pi_{\mathcal{F}}^k(v)), 0_{\mathcal{F}}))}_{=0} \\
&= \hat{a}_h(\underline{\boldsymbol{v}}_h, \underline{\hat{\boldsymbol{I}}}_h^k(v))\,.
\end{aligned}$$

In what follows, we consider that v and $v_{\mathcal{F}}$ are normalized in the sense $||v||_{\mathrm{L}} = ||v_{\mathcal{F}}||_{\mathrm{L}} = 1$. Next, we set $\mathfrak{J}_v := \hat{a}_h(\hat{\underline{\boldsymbol{I}}}_h^k(v), \hat{\underline{\boldsymbol{I}}}_h^k(v)) - a(v,v)$. Then, we deduce that

$$\begin{aligned}\hat{a}_h(\underline{\boldsymbol{v}}_h - \hat{\underline{\boldsymbol{I}}}_h^k(v), \underline{\boldsymbol{v}}_h - \hat{\underline{\boldsymbol{I}}}_h^k(v)) &= \hat{a}_h(\underline{\boldsymbol{v}}_h, \underline{\boldsymbol{v}}_h) - 2\,\hat{a}_h(\underline{\boldsymbol{v}}_h, \hat{\underline{\boldsymbol{I}}}_h^k(v)) + \hat{a}_h(\hat{\underline{\boldsymbol{I}}}_h^k(v), \hat{\underline{\boldsymbol{I}}}_h^k(v)) \\ &= (\lambda_h + 1)\left(||v_{\mathcal{F}}||_{\mathrm{L}}^2 - 2\,(v_{\mathcal{F}}, v)_{\mathrm{L}} + ||v||_{\mathrm{L}}^2\right) - (\lambda_h - \lambda)||v||_{\mathrm{L}}^2 + \mathfrak{J}_v \\ &= (\lambda_h + 1)\,||v_{\mathcal{F}} - v||_{\mathrm{L}}^2 - \lambda_h + \lambda + \mathfrak{J}_v\,. \end{aligned} \tag{32}$$

$\mathfrak{J}_v$ is bounded in analogous way as $\mathfrak{I}_{2,2}$ in the proof of Lemma 4.3 Then, after invoking Theorem 4.1, to bound the first two terms in (32), we derive (30). On the other hand, we notice that

$$\begin{aligned}||\nabla(v - p_h^{k+1}(\underline{\boldsymbol{v}}_h))||_{0,\Omega} &\leq ||\nabla_h(v - p_h^{k+1}(\hat{\underline{\boldsymbol{I}}}_h^k(v)))||_{0,\Omega} + ||\nabla_h\, p_h^{k+1}(\hat{\underline{\boldsymbol{I}}}_h^k(v)) - \underline{\boldsymbol{v}}_h))||_{0,\Omega} \\ &\leq ||\nabla_h(v - p_h^{k+1}(\hat{\underline{\boldsymbol{I}}}_h^k(v)))||_{0,\Omega} + \hat{a}_h(\underline{\boldsymbol{v}}_h - \hat{\underline{\boldsymbol{I}}}_h^k(v), \underline{\boldsymbol{v}}_h - \hat{\underline{\boldsymbol{I}}}_h^k(v))^{1/2}\,.\end{aligned}$$

Therefore, (31) is obtained after taking into account the approximation property of elliptic projector $p_h^{k+1}(\hat{\underline{\boldsymbol{I}}}_h^k(v))$ (cf. Theorem 1.48 in [25]) and (30). □

Remark 4.3 *We realize from Corollary 4.1 that if $s = k+1$, then we obtain the expected rates of superconvergence in this context: order h^{k+1} for the eigenfunctions in the H^1-seminorm, and $h^{2(k+1)}$ for the eigenvalues.*

Remark 4.4 *The case $\Gamma_{\mathtt{R}} = \emptyset$ can be covered by the described analysis, under certain appropriate adjustments. In this case, the resulting variational formulation is written as* (3)*, with $\alpha = 0$. It is known that 0 is an eigenvalue, with associated eigenspace $G_0 := \mathcal{P}_d^0(\Omega)$. The rest of eigenvalues form a positive increasing sequence of real numbers, finite-multiplicity, isolated, that diverges to infinity. Their corresponding eigenspaces lie in $H^{1+r}(\Omega)$, for some $r \geq 1/2$ (cf. Lemma 2.2 (ii) in [35]).*

Remark 4.5 *The current analysis can be adapted to cover the fully mixed Steklov eigenvalue problem: Find eingenpair (λ, u) such that*

$$\begin{cases} -\Delta u = 0 & \text{in} \quad \Omega \\ u = 0 & \text{on} \quad \Gamma_{\mathtt{D}} \\ \nabla u \cdot \boldsymbol{n} = \lambda\, u & \text{on} \quad \Gamma_{\mathtt{S}} \\ \nabla u \cdot \boldsymbol{n} = 0 & \text{on} \quad \Gamma_{\mathtt{N}} \\ \nabla u \cdot \boldsymbol{n} + \alpha\, u = 0 & \text{on} \quad \Gamma_{\mathtt{R}}\,, \end{cases} \tag{33}$$

where α is a non-negative constant function, and $\{\Gamma_{\mathtt{D}}, \Gamma_{\mathtt{S}}, \Gamma_{\mathtt{N}}, \Gamma_{\mathtt{R}}\}$ is a partition of the boundary $\Gamma := \partial\Omega$ with $|\Gamma_{\mathtt{D}}|, |\Gamma_{\mathtt{S}}| > 0$. In this case, it is not necessary to rewrite the boundary condition on $\Gamma_{\mathtt{S}}$ as (2)*, and we can block the HHO approximation of the trace on each edge F lying on $\Gamma_{\mathtt{D}}$ as usual (and fixed to be 0, for test and trial spaces).*

5 Numerical examples

The proposed numerical method was implemented in the open-source DiSk++ numerical library (`https://github.com/wareHHOuse/diskpp`) [18], which allows fast prototyping of discontinuous methods for PDEs. The discrete eigenvalue problem is solved using the FEAST algorithm [38, 31, 36] and using MUMPS [4, 5] as the underlying linear solver.

Concerning the variant (1) of the Steklov problem, we will present the results of HHO running on the test cases proposed in [34] (all with $\Gamma_{\mathtt{D}} = \emptyset$). Differently from [34] however, in addition to the cartesian meshes we will consider triangular and regular hexagonal tiling meshes in the 2D case (see Figure 1). In the 3D case we will consider tetrahedral meshes.

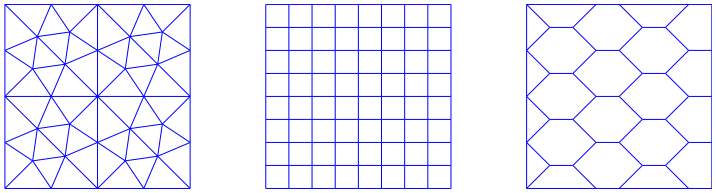

(a) Triangular (b) Cartesian (c) Hexagonal tiling

Figure 1: 2D polytopal meshes: triangular, cartesian, regular hexagonal tiling

5.1 Test 1: Sloshing problem

As in [34], our first test case is a sloshing problem [29], for which the analytical solution is known. In the 2D case, the problem setting and the corresponding analytical solution are given next

$$\begin{cases} \Omega := (0,1)^2\,,\ \Gamma_{\mathtt{S}} := \{(x,y)\,|\,0 \le x \le 1, y = 1\}\,,\ \Gamma_{\mathtt{D}} = \Gamma_{\mathtt{R}} := \emptyset\,,\ \Gamma_{\mathtt{N}} := \partial\Omega \setminus \Gamma_{\mathtt{S}}\,, \\ \lambda_n = n\pi\tanh(n\pi)\,,\ u_n(x,y) = \cos(n\pi x)\cosh(n\pi y)\,,\ n \in \mathbb{Z}_0^+\,. \end{cases}$$

We tested the convergence of our method for $k \in \{0,1,2\}$ on a sequence of triangular and cartesian meshes, in addition we tested the method also on a regular hexagonal tiling sequence of meshes from the FVCA5 benchmark [30]. The error and the convergence rate for the first four lowest positive eigenvalues is reported in Table 1 for triangles, in Table 2 for quadrangles and in Table 3 for regular hexagonal tiling. In all the cases we observe the optimal rate predicted by the theoretical results. We notice that the convergence rate of the first eigenvalue for the case k=2 is limited by the floating-point roundoff error.

	$\lvert\lambda_1 - \lambda_{1,h}\rvert$		$\lvert\lambda_2 - \lambda_{2,h}\rvert$		$\lvert\lambda_3 - \lambda_{3,h}\rvert$		$\lvert\lambda_4 - \lambda_{4,h}\rvert$	
$h/\sqrt{2}$	Error	Rate	Error	Rate	Error	Rate	Error	Rate
0.125	1.96E-02		1.60E-01		5.36E-01		1.25E+00	
0.0625	4.91E-03	2.00	4.03E-02	1.99	1.36E-01	1.98	3.21E-01	1.97
0.03125	1.23E-03	2.00	1.01E-02	2.00	3.40E-02	2.00	8.06E-02	1.99
0.015625	3.07E-04	2.00	2.52E-03	2.00	8.51E-03	2.00	2.02E-02	2.00
0.125	6.63E-04		1.65E-02		1.03E-01		3.46E-01	
0.0625	4.47E-05	3.89	1.20E-03	3.78	8.36E-03	3.62	3.25E-02	3.41
0.03125	2.89E-06	3.95	7.94E-05	3.92	5.70E-04	3.88	2.31E-03	3.81
0.015625	1.83E-07	3.98	5.07E-06	3.97	3.67E-05	3.96	1.50E-04	3.94
0.125	1.15E-06		1.51E-04		2.56E-03		1.90E-02	
0.0625	1.87E-08	5.95	2.36E-06	6.00	4.04E-05	5.99	3.02E-04	5.98
0.03125	2.70E-10	6.12	3.69E-08	6.00	6.31E-07	6.00	4.73E-06	6.00
0.015625	2.15E-11	3.65	5.67E-10	6.02	9.83E-09	6.00	7.37E-08	6.00

Table 1: Errors and computed convergence rates of first 4 lowest positive eigenvalues for Test 1, 2D (Triangles, with $k \in \{0,1,2\}$ from top to bottom).

Concerning the 3D case, the problem setting and the corresponding analytical solution are given next.

$$\begin{cases} \Omega := (0,1)^3\,,\ \Gamma_{\mathtt{S}} := \{(x,y,z)\,|\,0 \le x,y \le 1\,,\ z = 1\}\,,\ \Gamma_{\mathtt{R}} := \emptyset\,,\ \Gamma_{\mathtt{N}} := \partial\Omega \setminus \Gamma_{\mathtt{S}}\,, \\ \lambda_{m,n} = \ell\,\pi\ \tanh(\ell\,\pi), u_{m,n}(x,y) = \cos(m\,\pi\,x)\ \cos(n\,\pi\,y)\ \cosh(\ell\,\pi\,z)\,,\ \ell := \sqrt{m^2+n^2}\,, \quad m,n \in \mathbb{Z}_0^+\,. \end{cases}$$

	$\lvert\lambda_1 - \lambda_{1,h}\rvert$		$\lvert\lambda_2 - \lambda_{2,h}\rvert$		$\lvert\lambda_3 - \lambda_{3,h}\rvert$		$\lvert\lambda_4 - \lambda_{4,h}\rvert$	
h	Error	Rate	Error	Rate	Error	Rate	Error	Rate
0.0883883	7.42E-02		5.29E-01		1.55E+00		3.12E+00	
0.0441942	1.90E-02	1.96	1.46E-01	1.86	4.72E-01	1.72	1.06E+00	1.56
0.0220971	4.79E-03	1.99	3.74E-02	1.96	1.25E-01	1.92	2.92E-01	1.86
0.0110485	1.20E-03	2.00	9.42E-03	1.99	3.17E-02	1.98	7.49E-02	1.96
0.0883883	3.36E-04		1.21E-02		1.24E-01		1.15E+00	
0.0441942	1.97E-05	4.09	6.72E-04	4.17	5.33E-03	4.54	2.42E-02	5.57
0.0220971	1.28E-06	3.95	4.12E-05	4.03	3.16E-04	4.08	1.35E-03	4.17
0.0110485	7.98E-08	4.00	2.57E-06	4.01	1.95E-05	4.02	8.25E-05	4.03
0.0883883	2.32E-07		3.45E-05		1.27E-03		2.32E+00	
0.0441942	3.48E-09	6.06	4.58E-07	6.23	8.33E-06	7.26	6.89E-05	15.04
0.0220971	3.01E-11	6.85	6.84E-09	6.06	1.19E-07	6.12	9.16E-07	6.23
0.0110485	2.33E-12	3.69	1.04E-10	6.04	1.82E-09	6.04	1.37E-08	6.06

Table 2: Errors and computed convergence rates of first 4 lowest positive eigenvalues for Test 1, 2D (Cartesian meshes, with $k \in \{0, 1, 2\}$ from top to bottom).

We run the HHO scheme on a family of tetrahedral meshes that are a partition of $\bar{\Omega}$, and with uniform polynomial degree $k \in \{0, 1\}$. For $k = 0$, we set $\tau_{\partial T} := h_T^{-1}$. However, when $k = 1$ and considering the same parameter $\tau_{\partial T}$ as before, we notice the presence of spurious eigenvalues when solving the problem on the coarsest mesh. This situation has been also detected using a conforming virtual element method in [35], where the authors have been studied the variation of the corresponding stabilization parameter. In order to avoid this phenomenon, we take $\tau_{\partial T} := 10\, h_T^{-1}$ for $k = 1$. In Table 4 we display the computed error and convergence rate of the first 4 eigenvalues. We observe that the error behaves as $\mathcal{O}(h^{2(k+1)})$, as predicted by the theory.

5.2 Test 2: Fully Mixed Steklov eigenvalue problem on a polygonal domain

In this section we report the HHO results on another test case proposed in [34], for problem (33). In two dimensions, we set the problem such that

$$\Omega := (0,1)^2\,,\ \Gamma_{\mathtt{R}} := \{(x,y)\,|\,0 \le x \le 1\,,\ y = 0\}\,,\ \Gamma_{\mathtt{D}} = \Gamma_{\mathtt{N}} := \emptyset\,,\ \Gamma_{\mathtt{S}} := \partial\Omega \setminus \Gamma_{\mathtt{R}}\,,\ \alpha := 1\,,$$

while in three dimensions the setting is given next

$$\Omega := (0,1)^3\,,\ \Gamma_{\mathtt{R}} := \{(x,y,z)\,|\,0 \le x, y \le 1\,,\ z = 0\}\,,\ \Gamma_{\mathtt{D}} = \Gamma_{\mathtt{N}} := \emptyset\,,\ \Gamma_{\mathtt{S}} := \partial\Omega \setminus \Gamma_{\mathtt{R}}\,,\ \alpha := 1\,.$$

For this test case, no analytical solution is known. The stabilization parameter $\tau_{\partial T}$ is setting as h_T^{-1} in all cases presented here (2D and 3D). For the 2D setting, we report in Tables 5 and 6 the first 8 eigenvalues computed with HHO using $k = 0$ and $k = 2$, respectively, on triangular, quadrangular and regular hexagonal tiling meshes of similar size h. We notice from these tables, that the HHO method is convergent, since we obtain similar approximation of first 8 eigenvalues, using different kind of 2D-meshes, and approximation degrees $k \in \{0, 2\}$. Indeed, for $k = 2$ (cf. Table 6) we obtain better accuracy of approximation of eigenvalues, with 9-10 exact digit decimal places. On the other hand, this experiment gives us strong evidence of the robustness of the method (polytopal meshes and higher order). In addition, in Figure 2 the corresponding eigenfunctions are depicted, when approximation is obtained using hexagonal dominant meshes and $k = 2$.

	$\lvert\lambda_1 - \lambda_{1,h}\rvert$		$\lvert\lambda_2 - \lambda_{2,h}\rvert$		$\lvert\lambda_3 - \lambda_{3,h}\rvert$		$\lvert\lambda_4 - \lambda_{4,h}\rvert$	
$h/\sqrt{2}$	Error	Rate	Error	Rate	Error	Rate	Error	Rate
0.0906001	6.99E-02		2.64E+00		3.29E+00		4.58E+00	
0.0460523	1.74E-02	2.05	1.35E-01	4.39	4.33E-01	3.00	9.73E-01	2.29
0.0232271	4.46E-03	1.99	3.55E-02	1.95	1.17E-01	1.91	2.71E-01	1.87
0.0116655	1.13E-03	2.00	9.06E-03	1.98	3.03E-02	1.96	7.10E-02	1.94
0.0906001	1.31E-04		4.27E-03		3.69E-02		2.02E+00	
0.0460523	8.11E-06	4.11	2.61E-04	4.13	2.01E-03	4.30	8.65E-03	8.06
0.0232271	5.03E-07	4.06	1.61E-05	4.07	1.23E-04	4.08	5.23E-04	4.10
0.0116655	3.13E-08	4.03	1.00E-06	4.04	7.62E-06	4.04	3.22E-05	4.05
0.0906001	9.44E-08		1.34E-05		2.98E-04		1.92E+00	
0.0460523	1.45E-09	6.17	1.91E-07	6.28	3.41E-06	6.61	2.72E-05	16.50
0.0232271	2.24E-11	6.10	2.91E-09	6.11	5.04E-08	6.16	3.85E-07	6.22
0.0116655	4.53E-13	5.66	4.44E-11	6.07	7.74E-10	6.07	5.84E-09	6.08

Table 3: Errors and computed convergence rates of first 4 lowest positive eigenvalues for Test 1, 2D (Regular hexagonal tiling meshes, with $k \in \{0, 1, 2\}$ from top to bottom).

	$\lvert\lambda_{1,0} - \lambda_{1,0,h}\rvert$		$\lvert\lambda_{1,1} - \lambda_{1,1,h}\rvert$		$\lvert\lambda_{0,2} - \lambda_{0,2,h}\rvert$		$\lvert\lambda_{2,2} - \lambda_{2,2,h}\rvert$	
h	Error	Rate	Error	Rate	Error	Rate	Error	Rate
0.221721	5.63E-02		1.34E-01		3.96E-01		5.66E-01	
0.112285	1.48E-02	1.97	3.49E-02	1.97	1.05E-01	1.96	1.45E-01	2.00
0.0570394	3.83E-03	1.99	9.07E-03	1.99	2.73E-02	1.98	3.80E-02	1.98
0.221721	2.44E-04		1.13E-03		5.83E-03		1.13E-02	
0.112285	1.61E-05	3.99	7.47E-05	4.00	4.16E-04	3.88	8.09E-04	3.88
0.0570394	1.08E-06	4.00	4.96E-06	4.00	2.77E-05	4.00	5.42E-05	3.99

Table 4: Errors and computed convergence rates of first 4 lowest positive eigenvalues for Test 1, 3D (Tetrahedral meshes, with $k \in \{0, 1\}$ from top to bottom).

Concerning the 3D case, in Table 7 we report the numerical approximation of the first 8 lowest eigenvalues of the proposed problem, using HHO with $k = 0$, and considering a tetrahedral mesh of size $h = 0.112285$. Here, we notice that the approximations of eigenvalues are in agreement to the corresponding ones, obtained using HDG in [34]. The 8 eigenfunctions associated to each one of the estimated eigenvalues are displayed in Figure 3.

5.3 Test 3: Fully Mixed Steklov eigenvalue problem on a non-polygonal domain

This case has been taken again from [34], to test problem (33), and consider the domain is the unit disk or sphere. The specifications of the geometric data are given next

$$\text{2D:} \begin{cases} \Omega := \{(x,y) \in \mathbb{R}^2 \,|\, x^2 + y^2 < 1\}\,, \\ \Gamma_{\mathtt{R}} := \{(x,y) \in \mathbb{R}^2 \,|\, x^2 + y^2 = 1\,,\; y < 0\}\,, \Gamma_{\mathtt{D}} = \Gamma_{\mathtt{N}} := \emptyset\,, \Gamma_{\mathtt{S}} := \partial\Omega \setminus \Gamma_{\mathtt{R}}\,, \alpha := 1\,, \end{cases}$$

$$\text{3D:} \begin{cases} \Omega := \{(x,y,z) \in \mathbb{R}^3 \,|\, x^2 + y^2 + z^2 < 1\}\,, \\ \Gamma_{\mathtt{R}} := \{(x,y,z) \in \mathbb{R}^3 \,|\, x^2 + y^2 + z^2 = 1\,,\; z < 0\}\,, \Gamma_{\mathtt{D}} = \Gamma_{\mathtt{N}} := \emptyset\,, \Gamma_{\mathtt{S}} := \partial\Omega \setminus \Gamma_{\mathtt{R}}\,, \alpha := 1\,. \end{cases}$$

We point out that the analytical solution is not known in this case, neither for 2D nor 3D setting. Again, the penalization parameter is given by $\tau_{\partial T} := h_T^{-1}$.

Shape	h	λ_1	λ_2	λ_3	λ_4
Tri	0.0220971	0.2158345987	1.559895634	2.437819931	3.049920666
Cart	0.0220971	0.2158221562	1.559731073	2.43559051	3.048602022
Hex	0.0232271	0.2158325602	1.559368485	2.436442895	3.046759849
		λ_5	λ_6	λ_7	λ_8
Tri	0.0220971	4.709098557	5.630192912	5.701706322	7.838072639
Cart	0.0220971	4.699926448	5.611148065	5.683806583	7.79151958
Hex	0.0232271	4.696807926	5.611199255	5.680990839	7.785458602

Table 5: Comparison of the agreement of approximation of first 8 lowest eigenvalues on different mesh shapes (Test 2, 2D, with $k = 0$).

Shape	h	λ_1	λ_2	λ_3	λ_4
Tri	0.03125	0.2158385026	1.559903017	2.438500603	3.050532108
Cart	0.02209	0.2158385026	1.559903017	2.438500603	3.050532108
Hex	0.02323	0.2158385026	1.559903017	2.438500603	3.050532108
		λ_5	λ_6	λ_7	λ_8
Tri	0.03125	4.711999675	5.636832636	5.708207711	7.853979883
Cart	0.02209	4.711999678	5.636832650	5.708207724	7.853980005
Hex	0.02323	4.711999678	5.636832652	5.708207726	7.853980022

Table 6: Comparison of the agreement of approximation of first 8 lowest eigenvalues on different mesh shapes (Test 2, 2D, with $k = 2$).

λ_1	λ_2	λ_3	λ_4
0.1366378544	1.19685572	1.197515884	1.631688662
λ_5	λ_6	λ_7	λ_8
1.731891951	2.205594584	2.208357933	2.580903701

Table 7: Approximation of first 8 lowest eigenvalues using a tetrahedral mesh with $h = 0.112285$ (Test 2, 3D, with $k = 0$).

λ_1	λ_2	λ_3	λ_4
0.37282978	1.500432481	2.380894889	3.39876627
λ_5	λ_6	λ_7	λ_8
4.346537437	5.354953316	6.321283502	7.324445868

Table 8: Approximation of first 8 lowest eigenvalues using a triangular mesh with size $h = 0.0220536$ (Test 3, 2D, with $k = 0$).

λ_1	λ_2	λ_3	λ_4
0.3874486785	1.507367911	1.507385913	2.322542316
λ_5	λ_6	λ_7	λ_8
2.567800877	2.567884983	3.371264507	3.371595896

Table 9: Approximation of first 8 lowest eigenvalues using a tetrahedral mesh with size $h = 0.11256$ (Test 3, 3D, with $k = 0$).

k	λ_1	λ_2	λ_3	λ_4
0	0.3724394903	1.498532641	2.373266412	3.377001344
1	0.3728902032	1.500810900	2.381332254	3.399168194
2	0.3729548393	1.501152576	2.382297588	3.401400182
k	λ_5	λ_6	λ_7	λ_8
0	4.302096783	5.269212138	6.177973525	7.100710751
1	4.345851994	5.352344733	6.311914181	7.300377389
2	4.350892958	5.361984031	6.331864688	7.339754829

Table 10: Test 3 (2D): First 8 eigenvalues computed on a triangular mesh of size $h = 0.1$.

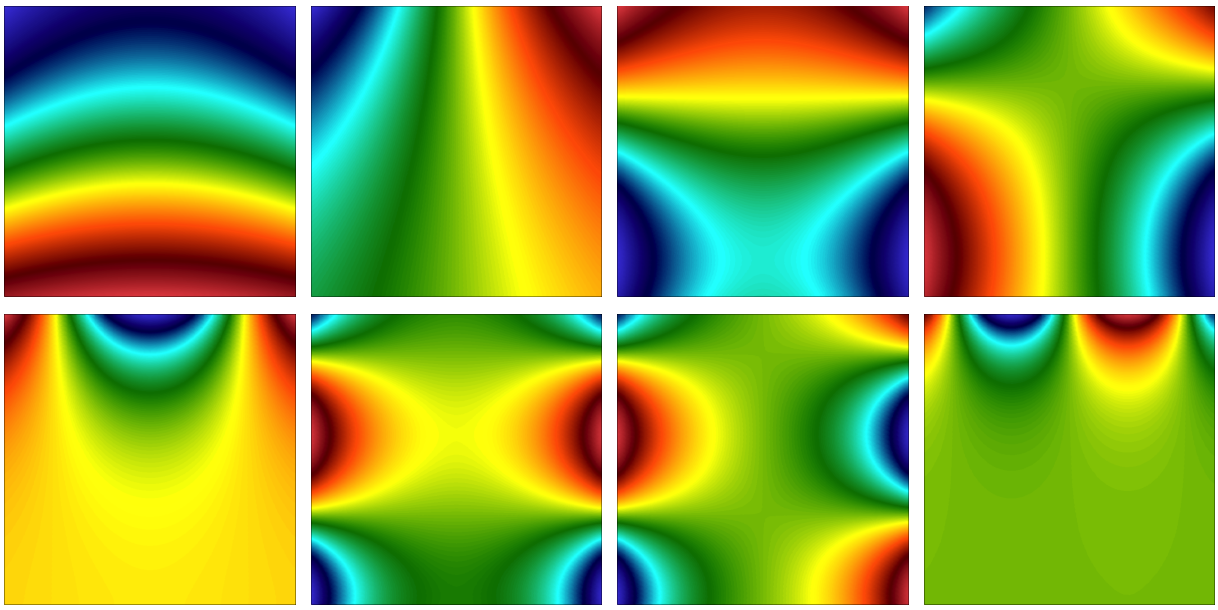

Figure 2: Numerical approximation of first 8 eigenfunctions of Test 2 (2D), with $k = 2$.

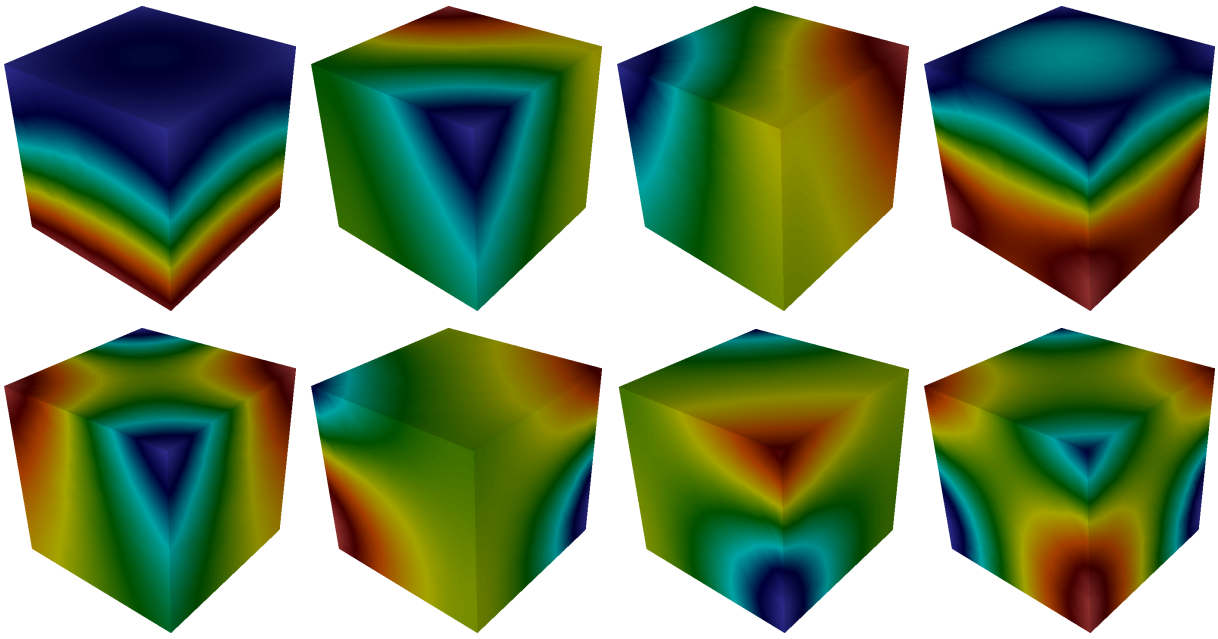

Figure 3: Numerical approximation of first 8 eigenfunctions of Test 2 (3D), with $k = 0$.

k	λ_1	λ_2	λ_3	λ_4
0	0.3870775984	1.505550727	1.505617868	2.313113187
1	0.3878616186	1.509634057	1.509703750	2.329887643
2	0.3879830610	1.510166664	1.510222522	2.331344420
k	λ_5	λ_6	λ_7	λ_8
0	2.556501707	2.556761039	3.340508093	3.341559915
1	2.576496110	2.576675517	3.391642341	3.392248521
2	2.577863626	2.578037715	3.395138790	3.395765921

Table 11: Test 3 (3D): First 8 eigenvalues computed on a tetrahedral mesh of size $h = 0.18$.

Concerning the 2D case, in Table 10, we report the first 8 lowest eigenvalues computed with HHO using $k \in \{0, 1, 2\}$ on triangular mesh of size $h = 0.1$. In addition, in Figure 4 the corresponding eigenfunctions, for $k = 2$, are depicted. On the other hand, for the 3D setting, we display in Table 11 the first 8 lowest eigenvalues computed with HHO with $k \in \{0, 1, 2\}$, using a tetrahedral mesh of size $h = 0.18$. The corresponding eigenfunctions, considering $k = 2$, are shown in Figure 5 . Despite the fact that the size of the considered meshes are not small enough, we notice that in both cases the method is convergent.

In Tables 8 and 9, we report the approximation of the first 8 lowest eigenvalues of problem (33) in 2D and 3D, respectively, considering $k = 0$ in both situations, and on finer meshes. The results are in agreement with the ones obtained using HDG method with $k = 0$ (see [34]).

Conclusions

We have extended the application of HHO method to Steklov-type eigenvalue problems. The key idea, for the analysis, relies on the deduction of a suitable sequence of finite-rank discrete solver operators, which helps us to invoke well known results of spectral theory of compact operators [8]. As a result,

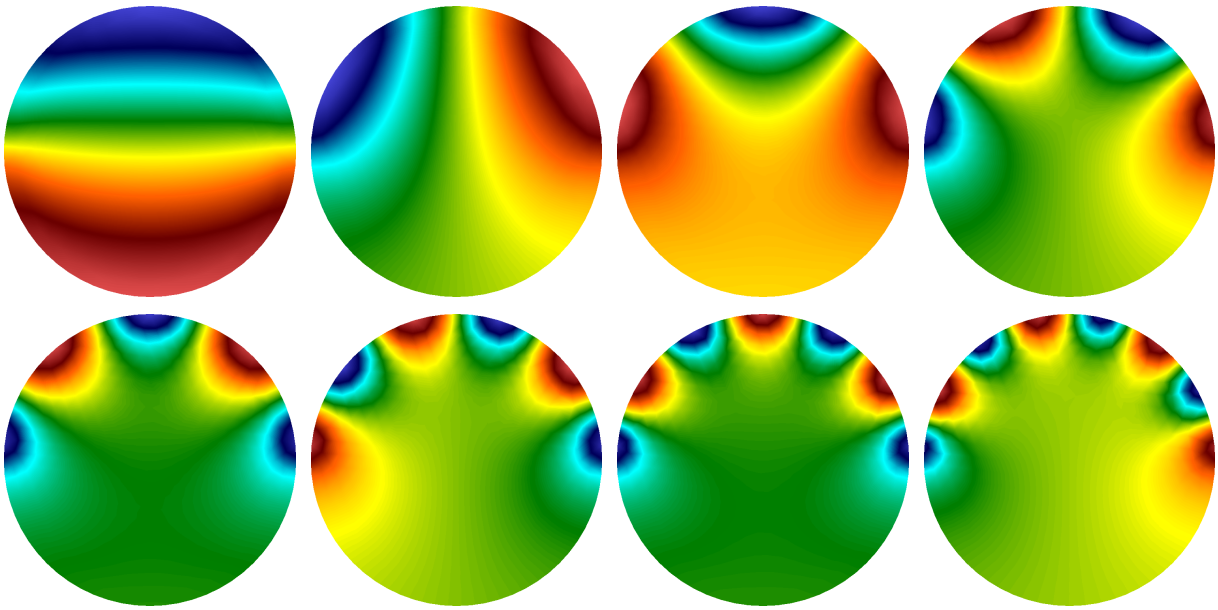

Figure 4: Test 3 (2D): First 8 eigenfunctions on unit disk ($k = 2$)

we have proved that the approximation of eigenvalues converge to the exact ones as $h^{2(k+1)}$, when piecewise polynomial of degree at most k are considered for approximating smooth eigenfunctions. Numerical examples are in agreement with our theoretical results, even in situations not covered by the current analysis (non polygonal domains). In addition, our results show evidence of the robustness of the method when using different type of polytopal meshes and high order degree.

Acknowledgements

Rommel Bustinza has been partially supported by ANID-Chile through FONDECYT grant 1200051. Matteo Cicuttin is member of INdAM-GNCS (Istituto Nazionale di Alta Matematica - Gruppo Nazionale per il Calcolo Scientifico), Italy. Ariel L. Lombardi is member of CONICET (Consejo Nacional de Investigaciones Científicas y Técnicas), Argentina. All authors have contributed equally in this article.

Appendix

The purpose here is to establish a discrete trace inequality result for functions belonging to $\underline{\boldsymbol{U}}_h^k$. To this aim, we assume for simplicity that $\mathcal{T}_h$ is made of simplicial cells. The general case can be derived following the ideas described in Section 6.5 in [25]. First, we recall that given $\underline{\boldsymbol{v}}_h := ((v_T)_{T\in\mathcal{T}_h}, (v_F)_{F\in\mathcal{F}_h^{\mathtt{skel}}}) \in \underline{\boldsymbol{U}}_h^k$, we set $v_h \in \mathcal{P}_d^k(\mathcal{T}_h)$ such that $\forall\, T \in \mathcal{T}_h \,:\, v_h|_T := v_T$. Other ingredient that will be useful is the operator $\underline{\boldsymbol{\pi}}_h : \underline{\boldsymbol{U}}_h^k \to \underline{\boldsymbol{U}}_h^0$, introduced in [25] (cf. (6.85)).

Lemma 5.1 *There exists $C_{\mathtt{tr}} > 0$, idependent of the mesh size, such that*

$$\forall\, \underline{\boldsymbol{u}}_h \in \underline{\boldsymbol{U}}_h^k \,:\, ||\gamma_h(\underline{\boldsymbol{u}}_h)||_{0,\Gamma} \,\leq\, C_{\mathtt{tr}}\, ||\underline{\boldsymbol{u}}_h||_h\,. \tag{34}$$

Proof. *We let $\underline{\boldsymbol{u}}_h \in \underline{\boldsymbol{U}}_h^k$ be fixed. Next, we introduce $\underline{\boldsymbol{z}}_h := \underline{\boldsymbol{u}}_h - \underline{\boldsymbol{\pi}}_h\underline{\boldsymbol{u}}_h \in \underline{\boldsymbol{U}}_h^{k,0} := \{\underline{\boldsymbol{v}}_h \in \underline{\boldsymbol{U}}_h^k \,:$*

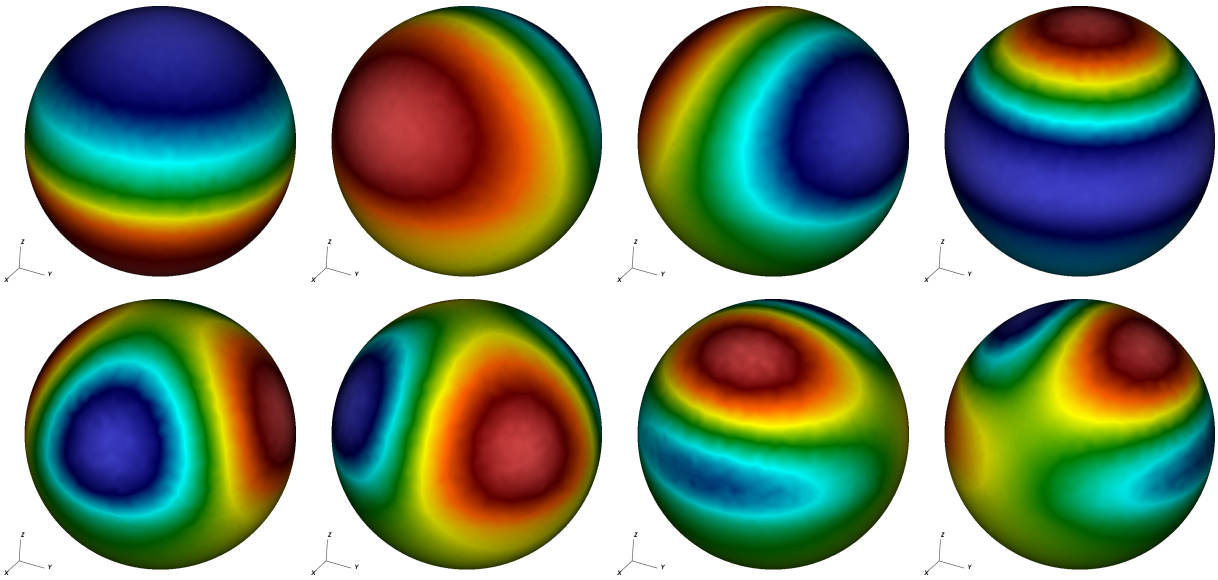

Figure 5: Test 3 (3D): First 8 eigenfunctions on unit sphere $(k = 2)$

$(v_h, 1)_{0,\Omega} = 0\}$. *Then, after invoking Theorem 6.7 and Lemma 6.38 in [25], we obtain*

$$\begin{aligned} ||\gamma_h(\underline{\boldsymbol{u}}_h)||_{0,\Gamma} &\leq ||\gamma_h(\underline{\boldsymbol{z}}_h)||_{0,\Gamma} + ||\gamma_h(\underline{\boldsymbol{\pi}}_h\underline{\boldsymbol{u}}_h)||_{0,\Gamma} \\ &\leq C_1 \,|\!|\!|\underline{\boldsymbol{z}}_h|\!|\!|_h + C_2 \,|\!|\!|\underline{\boldsymbol{\pi}}_h\underline{\boldsymbol{u}}_h|\!|\!|_h \\ &\leq C_1 \,|\!|\!|\underline{\boldsymbol{u}}_h|\!|\!|_h + (C_1 + C_2) \,|\!|\!|\underline{\boldsymbol{\pi}}_h\underline{\boldsymbol{u}}_h|\!|\!|_h \,. \end{aligned}$$

Therefore, thanks to the boundedness of $\underline{\boldsymbol{\pi}}_h$ *(cf. Lemma 6.33 in [25]), and the fact that* $|\!|\!|\cdot|\!|\!|_h \leq ||\cdot||_h$*, we establish* (34) *and we end the proof.* □

References

[1] ABBAS, M., ERN, A., AND PIGNET, N. Hybrid High-Order methods for finite deformations of hyperelastic materials. *Computational Mechanics 62*, 4 (2018), 909–928.

[2] ABBAS, M., ERN, A., AND PIGNET, N. A Hybrid High-Order method for incremental associative plasticity with small deformations. *Computer Methods in Applied Mechanics and Engineering 346* (2019), 891–912.

[3] ABBAS, M., ERN, A., AND PIGNET, N. A Hybrid High-Order method for finite elastoplastic deformations within a logarithmic strain framework. *International Journal for Numerical Methods in Engineering 120*, 3 (2019), 303–327.

[4] AMESTOY, P. R., DUFF, I. S., KOSTER, J., AND L'EXCELLENT, J.-Y. A fully asynchronous multifrontal solver using distributed dynamic scheduling. *SIAM Journal on Matrix Analysis and Applications 23*, 1 (2001), 15–41.

[5] AMESTOY, P. R., GUERMOUCHE, A., L'EXCELLENT, J.-Y., AND PRALET, S. Hybrid scheduling for the parallel solution of linear systems. *Parallel Computing 32*, 2 (2006), 136–156.

[6] ANDREEV, A. B., AND TODOROV, T. D. Isoparametric finite-element approximation of a Steklov eigenvalue problem. *IMA Journal of Numerical Analysis 24*, 2 (2004), 309–322.

[7] AYUSO DE DIOS, BLANCA, LIPNIKOV, KONSTANTIN, AND MANZINI, GIANMARCO. The nonconforming virtual element method. *ESAIM: Mathematical Modelling and Numerical Analysis 50*, 3 (2016), 879–904.

[8] BABUŠKA, I., AND OSBORN, J. Eigenvalue problems. In *Handbook of numerical analysis, Vol. II*, vol. II of *Handb. Numer. Anal.* North-Holland, Amsterdam, 1991, pp. 641–787.

[9] BERMÚDEZ, A., RODRÍGUEZ, R., AND SANTAMARINA, D. A finite element solution of an added mass formulation for coupled fluid-solid vibrations. *Numerische Mathematik 87*, 2 (2000), 201–227.

[10] BRAMBLE, J., AND OSBORN, J. Approximation of steklov eigenvalues of non-selfadjoint second order elliptic operators. In *The Mathematical Foundations of the Finite Element Method with Applications to Partial Differential Equations*, A. Aziz, Ed. Academic Press, 1972, pp. 387–408.

[11] BURMAN, E., DELAY, G., AND ERN, A. An unfitted hybrid high-order method for the Stokes interface problem. *IMA Journal on Numerical Analysis 41*, 4 (2021), 2362–2387.

[12] BURMAN, E., DURAN, O., AND ERN, A. Hybrid high-order methods for the acoustic wave equation in the time domain. *Communications on Applied Mathematics and Computation 4* (2022), 567–633.

[13] BURMAN, E., DURAN, O., ERN, A., AND STEINS, M. Convergence analysis of hybrid high-order methods for the wave equation. *Journal of Scientific Computing 87*, 3 (2021), Paper No. 91, 30.

[14] CALO, V., CICUTTIN, M., DENG, Q., AND ERN, A. Spectral approximation of elliptic operators by the hybrid high-order method. *Mathematics of Computation 88*, 318 (2019), 1559–1586.

[15] CASCAVITA, K. L., BLEYER, J., CHATEAU, X., AND ERN, A. Hybrid discretization methods with adaptive yield surface detection for Bingham pipe flows. *Journal of Scientific Computing 77*, 3 (2018), 1424–1443.

[16] CASCAVITA, K. L., CHOULY, F., AND ERN, A. Hybrid high-order discretizations combined with Nitsche's method for Dirichlet and Signorini boundary conditions. *IMA Journal of Numerical Analysis 40*, 4 (2020), 2189–2226.

[17] CHAVE, F., DI PIETRO, D. A., AND LEMAIRE, S. A discrete Weber inequality on three-dimensional hybrid spaces with application to the HHO approximation of magnetostatics. *Mathematical Models and Methods in Applied Sciences 32*, 01 (2022), 175–207.

[18] CICUTTIN, M., DI PIETRO, D. A., AND ERN, A. Implementation of Discontinuous Skeletal methods on arbitrary-dimensional, polytopal meshes using generic programming. *Journal of Computational and Applied Mathematics 344* (2018), 852–874.

[19] CICUTTIN, M., ERN, A., AND GUDI, T. Hybrid high-order methods for the elliptic obstacle problem. *Journal of Scientific Computing 83*, 1 (2020), Paper No. 8, 18.

[20] CICUTTIN, M., AND GEUZAINE, C. Numerical investigation of a 3d hybrid high-order method for the indefinite time-harmonic maxwell problem. *Finite Elements in Analysis and Design 233* (2024), 104124.

[21] COCKBURN, B. Static condensation, hybridization, and the devising of the hdg methods. In *Building Bridges: Connections and Challenges in Modern Approaches to Numerical Partial Differential Equations*, G. R. Barrenechea, F. Brezzi, A. Cangiani, and E. H. Georgoulis, Eds. Springer International Publishing, Cham, 2016, pp. 129–177.

[22] COCKBURN, B., DI PIETRO, D. A., AND ERN, A. Bridging the Hybrid High-Order and Hybridizable Discontinuous Galerkin Methods. *ESAIM: Mathematical Modelling and Numerical Analysis 50* (2015).

[23] COCKBURN, B., GOPALAKRISHNAN, J., AND LAZAROV, R. Unified hybridization of discontinuous Galerkin, mixed, and continuous Galerkin methods for second order elliptic problems. *SIAM Journal on Numerical Analysis 47*, 2 (2009), 1319–1365.

[24] COCKBURN, B., GOPALAKRISHNAN, J., AND SAYAS, F.-J. A projection-based error analysis of HDG methods. *Mathematics of Computation 79*, 271 (2010), 1351–1367.

[25] DI PIETRO, D. A., AND DRONIOU, J. *The hybrid high-order method for polytopal meshes*, vol. 19 of *MS&A. Modeling, Simulation and Applications*. Springer, Cham, 2020. Design, analysis, and applications.

[26] DI PIETRO, D. A., AND ERN, A. A Hybrid High-Order locking-free method for linear elasticity on general meshes. *Computer Methods in Applied Mechanics and Engineering 283* (2015), 1–21.

[27] DI PIETRO, D. A., ERN, A., AND LEMAIRE, S. An arbitrary-order and compact-stencil discretization of diffusion on general meshes based on local reconstruction operators. *Computational Methods in Applied Mathematics 14*, 4 (2014), 461–472.

[28] EVANS, D., AND MCIVER, P. Resonant frequencies in a container with a vertical baffle. *Journal of Fluid Mechanics 175* (1987), 295–307.

[29] FOX, D. W., AND KUTTLER, J. R. Sloshing frequencies. *Zeitschrift für angewandte Mathematik und Physik 34* (1983), 668–696.

[30] HERBIN, R., AND HUBERT, F. Benchmark on Discretization Schemes for Anisotropic Diffusion Problems on General Grids. In *Finite volumes for complex applications V* (France, June 2008), ISTE, Ed., Wiley, pp. 659–692.

[31] KESTYN, J., KALANTZIS, V., POLIZZI, E., AND SAAD, Y. Pfeast: A high performance sparse eigenvalue solver using distributed-memory linear solvers. In *SC '16: Proceedings of the International Conference for High Performance Computing, Networking, Storage and Analysis* (2016), pp. 178–189.

[32] LIU, J., SUN, J., AND TURNER, T. Spectral indicator method for a non-selfadjoint steklov eigenvalue problem. *Journal of Scientific Computing 79* (2019), 1814–1831.

[33] MGHAZLI, Z. Regularity of an elliptic problem with mixed Dirichlet-Robin boundary conditions in a polygonal domain. *Calcolo 29*, 3-4 (1992), 241–267.

[34] MONK, P., AND ZHANG, Y. An HDG method for the Steklov eigenvalue problem. *IMA Journal of Numerical Analysis 42*, 3 (2022), 1929–1962.

[35] MORA, D., RIVERA, G., AND RODRÍGUEZ, R. A virtual element method for the Steklov eigenvalue problem. *Mathematical Models and Methods in Applied Sciences 25*, 8 (2015), 1421–1445.

[36] PETER TANG, P. T., AND POLIZZI, E. Feast as a subspace iteration eigensolver accelerated by approximate spectral projection. *SIAM Journal on Matrix Analysis and Applications 35*, 2 (2014), 354–390.

[37] PLANCHARD, J., AND THOMAS, B. On the dynamical stability of cylinders placed in cross-flow. *Journal of Fluids and Structures 7*, 4 (1993), 321–339.

[38] POLIZZI, E. Density-matrix-based algorithm for solving eigenvalue problems. *Physical Review B 79* (2009), 115112.

[39] SAVARÉ, G. Regularity results for elliptic equations in Lipschitz domains. *Journal of Functional Analysis 152*, 1 (1998), 176–201.

[40] WANG, J., AND YE, X. A weak Galerkin finite element method for second-order elliptic problems. *Journal of Computational and Applied Mathematics 241* (2013), 103–115.